

PHYSICS OF SCRAP DISCRIMINATION

SEED PROJECT NUMBER: UX-1356

Final Report

November 24, 2004

Prepared for:

Strategic Environmental Research and Development Program
Arlington, VA 22203

Prepared by:

SIV Technologies Inc.
69 Main Street
Cherry Valley, MA 01611

Principal Investigator: Dr. D. A. Lieblich

Report Documentation Page				Form Approved OMB No. 0704-0188	
Public reporting burden for the collection of information is estimated to average 1 hour per response, including the time for reviewing instructions, searching existing data sources, gathering and maintaining the data needed, and completing and reviewing the collection of information. Send comments regarding this burden estimate or any other aspect of this collection of information, including suggestions for reducing this burden, to Washington Headquarters Services, Directorate for Information Operations and Reports, 1215 Jefferson Davis Highway, Suite 1204, Arlington VA 22202-4302. Respondents should be aware that notwithstanding any other provision of law, no person shall be subject to a penalty for failing to comply with a collection of information if it does not display a currently valid OMB control number.					
1. REPORT DATE 24 NOV 2004		2. REPORT TYPE Final		3. DATES COVERED -	
4. TITLE AND SUBTITLE Physics of Scrap Discrimination				5a. CONTRACT NUMBER	
				5b. GRANT NUMBER	
				5c. PROGRAM ELEMENT NUMBER	
6. AUTHOR(S) Dr. D. A. Lieblich				5d. PROJECT NUMBER UX-1356	
				5e. TASK NUMBER	
				5f. WORK UNIT NUMBER	
7. PERFORMING ORGANIZATION NAME(S) AND ADDRESS(ES) SIV Technologies Inc. 69 Main Street Cherry Valley, MA 01611				8. PERFORMING ORGANIZATION REPORT NUMBER	
9. SPONSORING/MONITORING AGENCY NAME(S) AND ADDRESS(ES) Strategic Environmental Research & Development Program 901 N Stuart Street, Suite 303 Arlington, VA 22203				10. SPONSOR/MONITOR'S ACRONYM(S) SERDP	
				11. SPONSOR/MONITOR'S REPORT NUMBER(S)	
12. DISTRIBUTION/AVAILABILITY STATEMENT Approved for public release, distribution unlimited					
13. SUPPLEMENTARY NOTES The original document contains color images.					
14. ABSTRACT					
15. SUBJECT TERMS					
16. SECURITY CLASSIFICATION OF:			17. LIMITATION OF ABSTRACT UU	18. NUMBER OF PAGES 52	19a. NAME OF RESPONSIBLE PERSON
a. REPORT unclassified	b. ABSTRACT unclassified	c. THIS PAGE unclassified			

1	SUMMARY	3
2	BACKGROUND	4
3	OBJECTIVE	4
4	TECHNICAL APPROACH.....	4
	4.1.1 <i>Modeling and Theoretical Analysis</i>	6
	4.1.2 <i>Experimental Testing and Analysis.....</i>	6
5	INTRODUCTION.....	7
6	RESULTS	8
6.1	UXO MODELS.....	8
6.2	SCRAP MODELS.....	10
6.2.1	<i>Regular Ordnance Scrap (ROS).....</i>	10
6.2.2	<i>Irregular Ordnance Scrap (IROS).....</i>	11
6.3	NOISE-FREE DATA INVERSION RESIDUALS.....	13
6.3.1	<i>Residual Field Comparison</i>	13
6.3.2	<i>Field Decay</i>	18
6.4	NOISY DATA INVERSION RESIDUALS	19
6.4.1	<i>Sensor Noise</i>	19
6.4.2	<i>Positioning Noise.....</i>	20
6.4.3	<i>Sensor and Positioning Noise.....</i>	24
6.5	SAMPLING	26
6.5.1	<i>Sampling Density.....</i>	26
6.5.2	<i>Sampling Window.....</i>	35
6.5.3	<i>Spectral Analysis</i>	36
6.6	EXPERIMENTAL.....	37
6.6.1	<i>Targets.....</i>	37
6.6.2	<i>Setup</i>	38
6.6.3	<i>Data Collection.....</i>	39
6.6.4	<i>Data Inversion Residuals.....</i>	40
7	FINDINGS.....	47
8	CONCLUSIONS:.....	51
9	RECOMMENDATIONS:	52
10	REFERENCES.....	52

1 Summary

This effort has achieved its objective of evaluating the feasibility of near-field-physics as a means of discriminating against shallow scrap, in magnetic UXO investigations. In addition, and unexpectedly, the near-field character of UXO has been identified as also being useful for discriminating among different UXO. Modeling the full 3D geometrical complexity of an 80-mm projectile, 155-mm projectile, and 2 pieces of irregular scrap provided the theoretical magnetostatic data required to perform the evaluation of near-field contributions to the total fields of these targets. Removal of the dipole field component was accomplished by fitting a standard prolate spheroidal model to the data, and subtracting the resulting field. Residual fields were evaluated to determine if the non-dipole components are: measurable, of distinctive signature, enhanced in the scrap relative to the UXO, and robust to typical noise sources. Additionally, practical sampling considerations for these fields were investigated to permit field collection and validation of the numerical results. Finally, field data were collected and analyzed to validate the numerical results.

Modeling results using the full 3D geometrical complexity of an 80-mm projectile, 155-mm projectile, and 2 pieces of irregular scrap confirmed the richness of the magnetostatic-field (at depths of up to 3 body lengths) had not been previously exploited. Residual fields, obtained after subtraction of the fitted dipole fields at depths between .5 and 3.0 body lengths, showed that the non-dipole components of scrap and UXO are: measurable, distinctive in space and/or differ in amplitude, enhanced by as much as 10 times in the scrap relative to the UXO, and robust to typical noise sources that interfere individually or in combination. Specifically, these residual fields were found to be of quadrupolar character in terms of spatial expression and decay rate. The presence of such fields was predicted to arise in scrap, and possibly UXO, due to previously neglected broken symmetries. The quadrupolar components of scrap and UXO field-residuals have not been previously identified. Residual signatures provide sufficient distinguishing characteristics to enable a practical discrimination methodology: for example, the signatures of an intact 155 and a piece of scrap that is a substantial portion of its body were found to be noticeably different, raising the possibility of discriminating even between these closely related objects. Practical sampling requirements were found to be more stringent than those commonly employed in field investigations and this led to a possible explanation for why prior field investigations have not detected these fields: they were aliased. Sampling of the residual fields requires consideration of the smallest target at the shallowest depth and may require tradeoffs between field collection time and data quality. Such tradeoffs can be made on a site specific basis. At present, a discrimination methodology using the quadrupolar-type field would be best applied as a cued technology. The unexpected identification of quadrupolar-type fields of UXO further enhances the method's appeal as these fields potentially allow discrimination among different UXO, as well as between scrap and UXO. Field results from 2 UXO and 2 scrap items were found to be suggestive of quadrupolar-type residuals; however, positioning errors limited the extractable information: field validation of the numerical results remains an outstanding issue that may be resolved by further processing of existing data, and/or collection of new data. The prospects for further development of the near-field magnetostatic-discrimination method are excellent as the present investigation has considered what is likely the worst case for scrap discrimination: the non-dipole fields of UXO have likely been maximized by the orientation chosen.

2 Background

The development of a feasible method for discriminating against metallic scrap, the predominant component of the false alarm rate in subsurface UXO investigations, has proved to be an elusive goal, with current magnetic and electromagnetic methods. Current UXO site remediation costs are dominated by the false alarm rate, which frequently accounts for over 70% of the remediation costs. False alarms per UXO item are usually greater than 10 and sometimes, as high as 100 or more. We propose a systematic approach to the physical description of measured fields in terms of the neglected near-field effects in magnetic data. The specific interaction of these near-field effects with the properties of metallic scrap has not been previously recognized: we expect this interaction to provide a basis and methodology for discrimination against false alarms. We anticipate that these methods could reduce site remediation costs by more than 35%.

3 Objective

The objective of this research is to:

- Evaluate the possibility of discriminating against scrap occurring within the top foot of the soil using the hitherto unaccounted for physics of the near field, for magnetic UXO investigations.

4 Technical Approach

Evaluation of the possibility of discriminating against scrap, occurring within the top foot of the soil, will be accomplished using the hitherto unaccounted for physics of the near field, as applied to magnetic UXO investigations. The approach is innovative in that it seeks to reduce costs by recognizing and removing a specific subset of easily recognizable nonUXO signatures, instead of finding a means of distinguishing the set of UXO signatures from nonUXO signatures.

Our approach includes theoretical analysis and experimental validation. Our theoretical analysis incorporates the full geometric complexity of UXO and scrap to an extent not previously achieved, instead of relying upon simplified models, as in prior efforts. Experiments will provide initial evaluation of theoretical results on actual targets. The results obtained will begin to build a database, which can form the basis for scrap discrimination.

Our approach is novel in that it incorporates the physics of the near field, which has been considered irrelevant to the discrimination problem, for magnetic data, owing primarily to 1) an assumed small ratio of length to range for UXO and scrap; and 2) an assumed symmetry for the dipole model of UXO. The first assumption effectively places UXO in the far field and leaves only the dipole response, which is the only response currently, being modeled. For UXO, all extant models (points, lines, spheres, cylinders, and ellipsoids) obey the second assumption whereby:

- UXO exhibit axial symmetry about at least one axis
- UXO exhibit mirror symmetry about a plane perpendicular to that axis
- UXO exhibit field homogeneity over and within the UXO

These are not bad assumptions. Even though they are clearly violated by many UXO, it has been shown (Mcfee and Das, 1990) that the next higher term, the octupole term, in the multipole field expansion of the magnetostatic field, is generally negligible: its field decays with an exponent equal to 2 less than that of the dipole. For example, in magnetics, the dipole field decays as $(\text{range})^{-3}$ so the octupole decays as $(\text{range})^{-5}$.

The significant effect of field decay can be recognized by considering an object at 1 versus 3 length dimensions range from the sensor. It is easy to calculate that by 3 length dimensions range, the magnetic octupole has diminished to about .4% of its former amplitude (at 1 length dimension, about 48 dB loss) whereas the dipole has diminished to about 4% of its former amplitude (about 29 dB loss). The combination of faster octupole decay and the fact that UXO tested to date (McFee and Das, 1990) produce negligibly small magnetic octupole moments, even at close ranges, suggests that UXO represent good approximations to the assumptions (listed above), for magnetic moments. In general, the details of object geometry will determine partitioning of fields into the respective moments.

Now let's consider the other side of the coin: scrap. Scrap is generally irregular and therefore has neither an axis of symmetry nor a mirror plane and, its geometry may result in complex fields on its surface and interior. In addition, the depth range of the majority of scrap is generally restricted to the upper foot of soil (figure 1), and only scrap large enough to be UXO, within that range, is of interest. This means scrap with largest length dimension not smaller than 3 inches, the approximate length of a 20 mm, the smallest UXO, is of interest. Burial, even at the maximum depth of 1 foot, would still be only 4 length dimensions of the smallest scrap size of interest: this might be increased to 6 length dimensions (of the smallest scrap of interest) if the sensor height is allowed to be up to 6 inches above the ground surface. It turns out that there is yet another advantageous aspect that will aid in scrap discrimination using higher order moments: by violating the above assumptions, the quadrupole moment, which disappears from the highly symmetrical and regular models above, is expected to reappear. The advantage of this for discrimination is that the field decays with an exponent equal to 1 less than that of the dipole. For example, in magnetics, the dipole field decays like $(\text{range})^{-3}$ so the quadrupole field decays like $(\text{range})^{-4}$. This is significant and magnetics offers a particular advantage owing to the fact that the sensor is passive: the field decays more slowly than an active sensor such as EM. For example, at the same range (3 length dimensions) as above, the field of the magnetic quadrupole has decayed to 1.2% (about 38 dB loss) of its amplitude at 1 length dimension whereas the EM quadrupole has decayed to .04% (67 dB loss) of its amplitude. In fact, even the EM dipole field has decayed to .1% (57 dB loss) of its amplitude. Combined with the expected strong excitation of the higher order moments, by the irregular geometry of the scrap, the quadrupole moment is expected to provide sufficient data to discern relative enrichment of the NONDIPOLE response from scrap, compared to the dipole response. This relative enrichment can be expressed as a ratio and compared with the same ratio of UXO to quantify the relative enrichment. We anticipate a threshold of this ratio, above which scrap is clearly indicated. Further, if the limited results for UXO, indicating weak excitation of the higher moments, are corroborated for a wider class of UXO, we anticipate that this "discrimination threshold" will be applicable to a large percentage of

scrap in the upper foot. We recognize that there will be targets: which occur at small length / range ratios, even within this restricted depth range; which do not excite the higher moments sufficiently strongly to yield a discrimination capability; which interfere and produce spurious results, and; which may otherwise not be amenable to this type of analysis. These limitations have led us to assume 50% effectiveness in application.

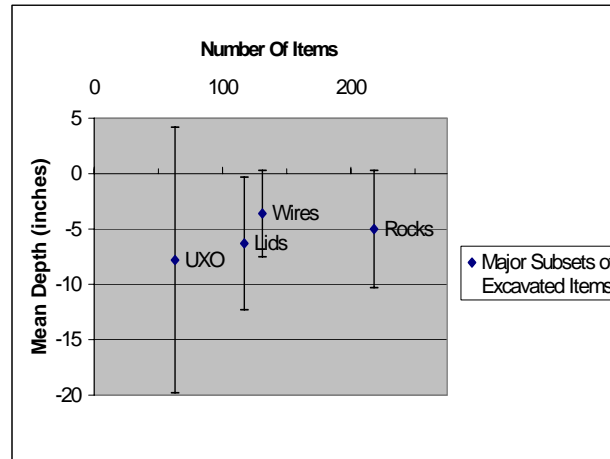


Figure 1. Scrap occurs primarily in the upper 1 foot of the soil. These data are from Umatilla Army depot (Lieblich, Reidy, and Foley, 1998). Bars indicate one standard deviation about the mean (point), assuming a symmetric Gaussian distribution. The vast majority of UXO and/or nonUXO scrap, at any site, occurs in the top 1 foot of the soil (Millhouse, 1998 pers. comm.)

4.1.1 Modeling and Theoretical Analysis

In this initial phase of the research, actual UXO and scrap shapes will be digitized, using the ORDATA data base and actual images of scrap fragments. Full field, modeling of the UXO and Scrap will yield signatures as functions of the many parameters which govern the detectability of higher moments. These signatures will be evaluated to determine if there are robust means of detecting the higher order contributions, under what circumstances this is feasible, and what field parameters need to be modified or developed to detect the higher order moment contribution (and enable discrimination).

4.1.2 Experimental Testing and Analysis

The theoretically determined constraints upon higher order moments will be tested using an accurately positioned handheld magnetic sensor. The sensor will be high resolution to obtain the maximal information of the higher order moments of the field. UXO measurements will expand the existing information on the ratio of higher order moments to the dipole moment, within UXO. The scrap data will determine these same characteristics for scrap and thereby provide the basis for differentiating scrap from UXO. The spatial expression of the residual field, after subtraction of the dipole field, will be compared to the theoretical model, to a quadrupole field, and to the noise, to discern if a meaningful discrimination can be accomplished. A quantitative characterization of the energy in the residual fields, compared to that in the dipole field will be made.

5 Introduction

The proposed discrimination methodology depends upon the differences between the non-dipole fields of scrap and UXO. Existing models were developed for UXO and hence employ significant simplifying assumptions about the nature of target geometry. Specifically, these models generally assume a prolate spheroidal shape for UXO. The prolate spheroidal shape is a special case of the spheroidal shape and the induced magnetostatic field at a point (x,y,z), for a spheroid at (x₀, y₀, z₀) can be written as (McFee and Das, 1990):

$$\vec{B} = \frac{\mu_0}{4\pi r^3} \left(\frac{3}{r^2} [\vec{r} \bullet \vec{M}] \vec{r} - \vec{M} \right) \quad (1)$$

where μ_0 is the magnetic permeability of free space, $r = \|\vec{r}\|$ is the distance of the measurement point from the center of the spheroid, and \vec{M} is the magnetic dipole moment. The magnetic dipole moment of a spheroid can be written as:

$$\vec{M} = \frac{V}{\mu_0} \overline{\overline{R}}^T \overline{\overline{D}} \overline{\overline{R}} \vec{B}_0 \quad (2)$$

where V is the volume of the spheroid, $\overline{\overline{R}}$ is the Euler rotation tensor from the geographic coordinate system to a body centered coordinate system, $\overline{\overline{D}}$ is the static demagnetization tensor, and \vec{B}_0 is the static magnetic field in geographic coordinates. $\overline{\overline{D}}$ is diagonal in the body centered coordinate system with one value corresponding to the symmetry axis and two equal values corresponding to the axes perpendicular to the symmetry axis. $\overline{\overline{D}}$ only depends upon the sizes of the spheroid axes (major axis 2a and minor axis 2c) and the relative magnetic permeability of the spheroid (μ_2) and the surrounding medium (μ_1).

Discrimination using the above model first requires fitting a parameterized model, $\vec{B}(x_0, y_0, z_0, M_x, M_y, M_z)$ being one such parameterization, to a set of field measurements collected over a permeable target. Discrimination could be achieved if there were a disparity in the fit of the model between sets of measurements collected over UXO and scrap. Unfortunately, the spheroidal model is versatile enough that it can generally be “force-fit” to the measured fields of UXO and scrap with equally good results (this has been minimized through the use of an unconstrained optimization for model parameters, in this effort). Additionally, as most scrap is not restricted to the spheroidal shape, the spheroidal assumption provides a poor approximation to the actual shape and results in effective- spheroidal parameters that are not representative of the object. These model considerations are added to the practical reality of measurement noise, which broadens the possible range of recovered parameters, and the inherent nonuniqueness of recovering the spheroidal model from its field, which yields a testing problem rather than an inversion. The result is that neither the goodness of fit, nor the parameters derived from the fit, provides sufficient capability to discriminate UXO from scrap, in general.

6 Results

The results of theoretical and experimental investigations of the non-dipole fields emanating from UXO and scrap are presented below. Theoretical results are presented first as these results laid the foundation for the experimental effort by defining the required parameters for measurement. Within the theoretical results, qualitative evaluation of the modeled fields is presented first, followed by quantitative inversion results, testing of noise effects, and finally, evaluation of sampling effects.

6.1 UXO Models

Two UXO were chosen for modeling: the 80-mm projectile within a U.S. cartridge, 120-mm, Heat-Mp-T, m830A1, penetrator and a 155-mm HE M101 projectile. Magnetic fields were calculated by solving Laplace's equation for a set of points lying on a plane, given a discrete 3D point-grid representation of a ferrous target, within the static field of the earth. The 80-mm projectile is substantially the same as the 81 mm modeled for electromagnetic purposes by Grimm (2001), however, the level of detail of the internal structure has not been previously modeled. The detail in the 80 mm projectile model, used for this evaluation, can be seen in figure 2.

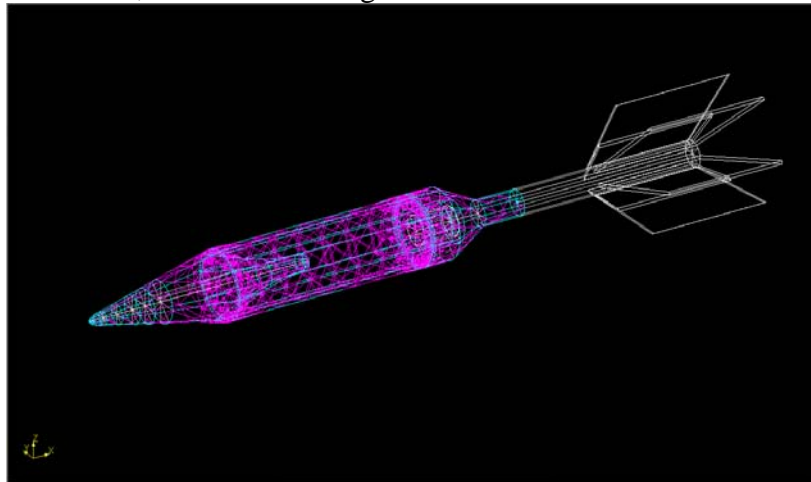


Figure 2. The 80 mm projectile model showing detailed external and internal structures. The fin assembly is aluminum and is therefore does not contribute to the magnetostatic modeling. The physical properties (denoted in blue) of the nose, body, and fin adapter have been assumed homogeneous owing to a lack of detailed information. The elements for numerical solution can be seen in pink.

Induced fields from this target were modeled in a vertical static field of 60,000 nT, with the target horizontal and with its long axis along the x direction. Modeling was completed at 5 different heights. An example of the results can be seen in the figure 3.

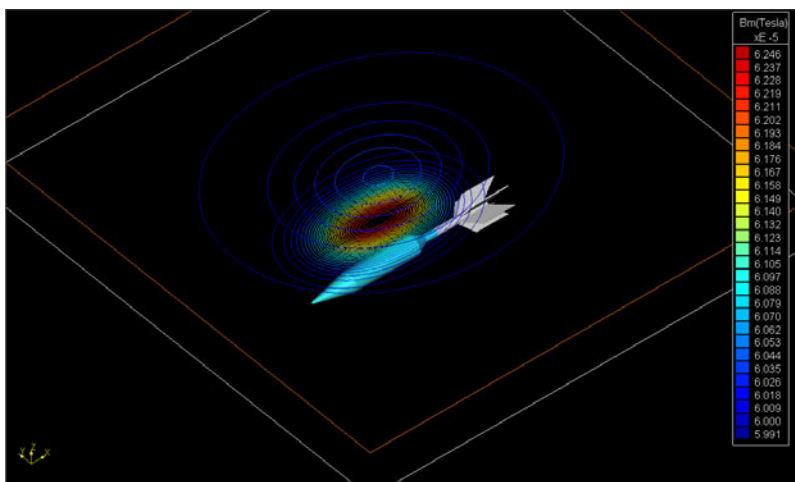


Figure 3. The field of a horizontal 80 mm projectile at 200 and 400 mm above the body (roughly one third and 3/4 of the 528 mm active body length (as compared to the 778 mm full body length), respectively) in a vertical field of 60,000 nT. The field of the UXO already appears to be substantially dipolar at the 400 mm level.

Similarly, modeling of the 155 HE M101 incorporated the detail of its geometry, as can be seen in figure 4. The internal structure of the 155 is less complex than the 80-mm, however, the exterior body has significant geometrical complexity, which includes the locations of the rotating bands. Although these were included in the model, they have essentially no effect on the magnetostatic fields.

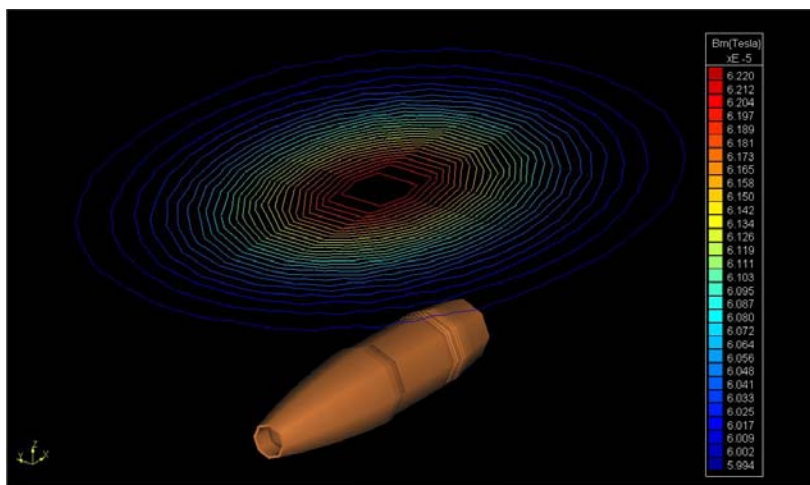


Figure 4. The 155 mm projectile model showing the plane at 38 cm above the horizontal shell. This corresponds to $\frac{1}{2}$ body length. The interior of the 155 mm is a hollow cylindrical structure, unlike the interior of the 81 mm projectile, modeled previously. Rotating bands are believed to be copper and are therefore not assigned in the magnetostatic model, although the actual geometry of the grooves within the shell is accurately represented (these grooves could be neglected as they have essentially no effect on the magnetostatic model). The physical properties (denoted in copper color) of the projectile have been assumed homogeneous owing to a lack of detailed information. The ambient field is a vertical field of 60,000 nT.

6.2 Scrap Models

Originally it was our intent to evaluate the non-dipole magnetic field of scrap derived from the UXO body and compare it to the intact UXO. As our geometric modeling progressed, we recognized that actual scrap could be divided into two predominant types, which we termed: regular and irregular, as described below. This subdivision of the scrap is consistent with the field excavation process, where notes often differentiate subcomponents of a UXO from OE scrap.

6.2.1 Regular Ordnance Scrap (ROS)

Regular ordnance-scrap (ROS), which we define as subcomponents of UXO, was modeled for the above 80-mm projectile. In contrast, the 155-mm projectile is a single piece of metal and cannot break into component pieces: it therefore contributes no ROS and was only modeled as IROS. We find that some subcomponents have stronger non-dipole signatures than others. Specifically, the field from the fin adaptor (figure 5) can be seen at about 1 body length above the assembly with an anomaly that has non-dipolar components whereas the nose section (figure 6) appears to be substantially dipolar at the same relative height. This was somewhat surprising as the exterior of the nose appears conical, however, this shape is substantially symmetric about a plane located perpendicular to the axis of the projectile and at the nose-body junction. As detailed physical properties for the sub-volumes were not available to us, they have been modeled as homogenous. Such information would further enhance our modeling results and might alter the some of the results, such as those for the nose of the 81-mm.

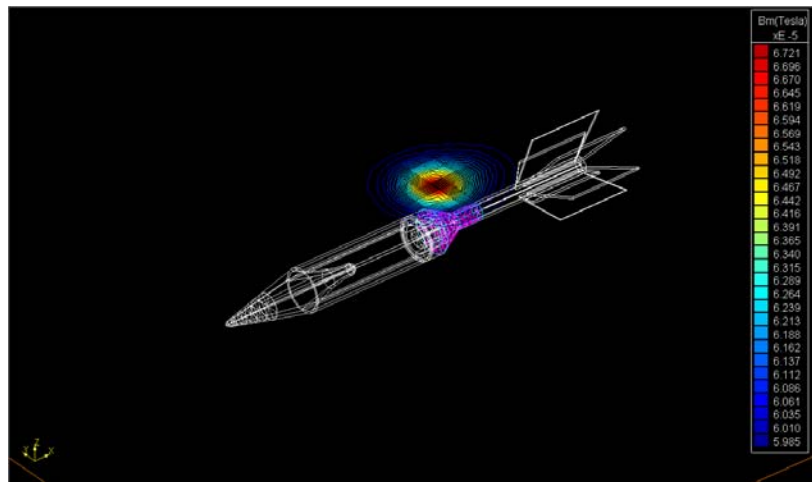


Figure 5. Fin adaptor of the 80 mm projectile modeled on the z-plane 87.5 mm above its axis (about one body length, 96 mm).

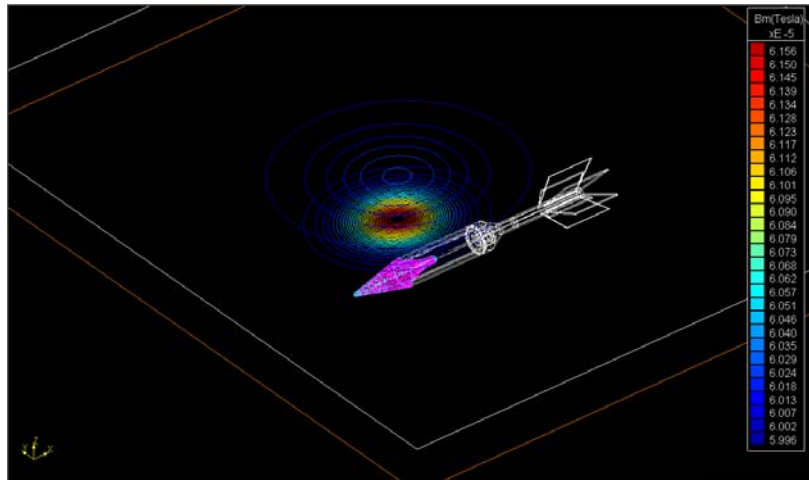


Figure 6. Nose assembly, including interior extension into the body. The actual model possesses more symmetry than would be expected by modeling the exterior alone. Two z-planes corresponding to heights of 175 and 310 mm (about half and 1 body length, actual is .6 and 1.1, of the 270 mm full body length) suggest that the field is substantially dipolar, even at half a body length. If detailed physical properties of this component differ from the assumed homogeneous steel, the symmetry may change dramatically, thereby altering the associated fields.

6.2.2 Irregular Ordnance Scrap (IROS)

Irregular ordnance-scrap (IROS), which we define to be exploded segments of the original shell, is the main focus of this investigation and two models have been generated, each derived from the original UXO model described above.

The first IROS model derives from the main body cylinder (275 mm) of the 80-mm projectile. It is less than half the cylinder length (119 mm) in its long dimension and has an arcuate extent of about 100° (figure 7). This segment of the UXO shows non-dipole components at 1 body length. Although this model represents a more realistic piece of scrap, it still possesses symmetries that are not generally present in actual scrap. We expect the non-dipole components in such geometries will be even more significant than those investigated here, thereby enhancing the discrimination capability of our method.

The second IROS model is derived from the 155 HE M101, previously modeled, and represents a significant portion of the body of that shell. This is important as presently there is no means of discriminating a large piece of a shell body from the actual full-shell. If, however, the non-dipole field of the large shell-piece is significantly enhanced compared to that of the full shell, owing to the decreased symmetry, a dig could be avoided on even a large piece of a shell. Accordingly, this model represents a piece of the body that is 500 mm long and is cut along an irregular surface that intersects the base of the shell near the center and becomes shallower as it progresses towards the front end, where it exits approximately 500 mm from the base (figure 8). An example of the field from this IROS can be seen in figure 9, at a depth of 1 body length.

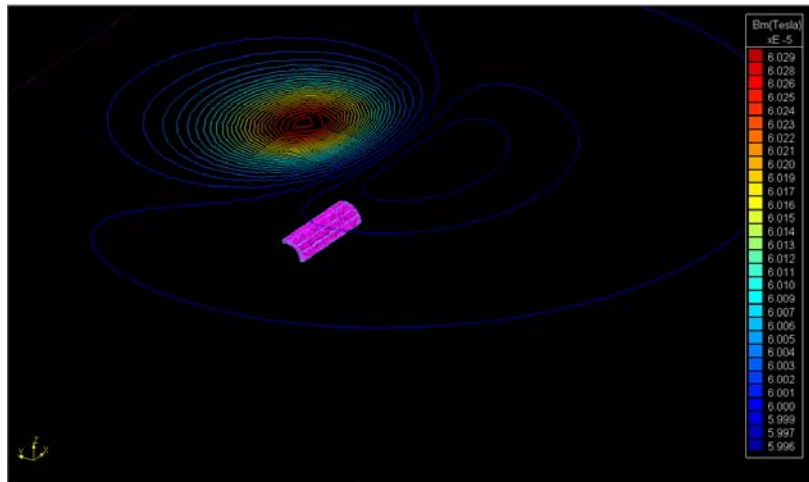


Figure 7. Irregular scrap represented by a section of the 80 mm body, approximately half the body length and covering about 100° of arc. A z-plane at about 1 body length above the target, in a vertical 60,000 nT field shows non-dipole components.

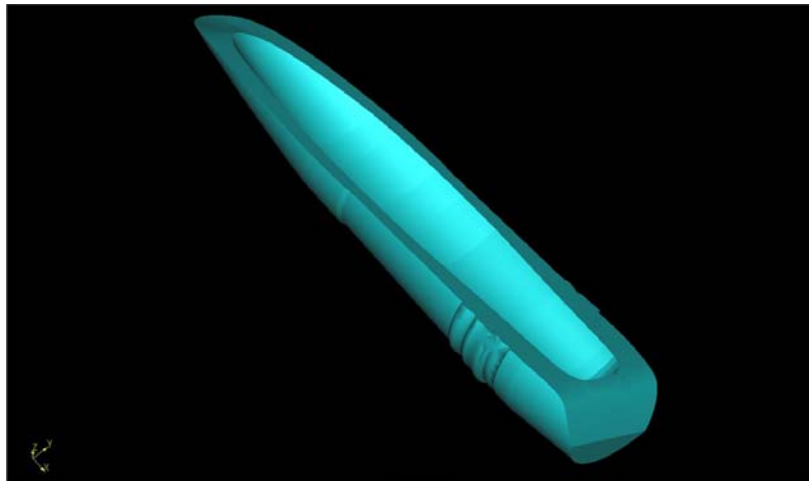


Figure 8. A cap-like sliver of irregular scrap from a 155 HE M101 used for modeling irregular scrap from this shell. The base of the shell is cut such that its thickest point is about 47 mm, less than the radius of a complete shell. Detailed external and internal structures can be seen in the model. The physical properties (denoted in blue have been assumed homogeneous owing to a lack of detailed information.

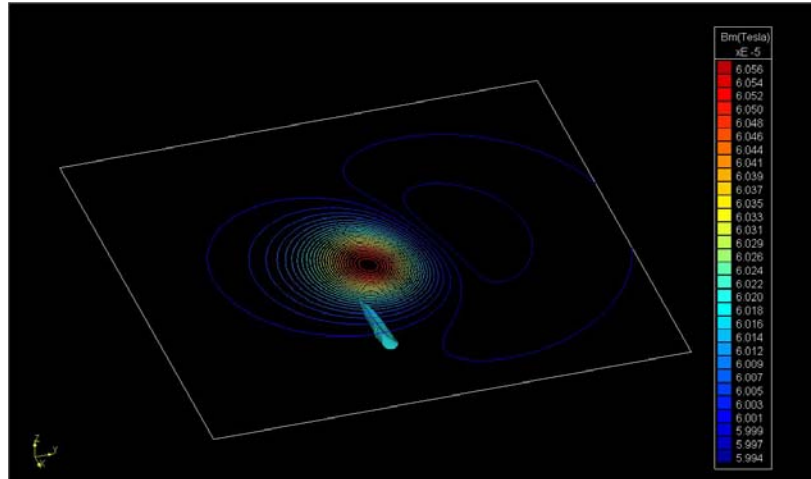


Figure 9. The field of the irregular scrap from the 155 HE M101 on a plane one body length (500 mm) above it, in a vertical field of 60,000 nT.

6.3 Noise-free Data Inversion Residuals

Quantitative evaluation of the presence of non-dipole fields requires elimination of the dipole field. This was the first goal of the inversion process. Additionally, results were obtained at different depths to determine the feasible depth to which the non-dipole fields might be measurable. Direct comparison of the fields from the UXO and the IROS provides quantitative information about the discriminatory capability of the non-dipole fields.

6.3.1 Residual Field Comparison

Full field models of IROS and UXO at depths ranging from .5 to 3.0 normalized depths (depth/body length) were used to evaluate the residual fields after inversion using the prolate spheroidal dipole model. Results are presented in figures 10-13. Each figure shows the IROS item in the left column, the UXO in the right, modeled field in the first row, fit field in the second row, and the residual in the last row. The range from .5 to 3.0 normalized depths is spanned by each pair of figures 10-11 and 12-13, the first being at .5 and the second at 3.0, respectively. Figures 10-11 cover the 80-mm UXO and it's IROS, while figures 12-13 cover the 155-mm and it's IROS. Direct comparisons of the absolute magnitudes and spatial signatures of the UXO and IROS residual fields are apparent in the last row of each figure. The first and third rows provide a comparison of the residual to the total field. These figures provide quantitative absolute and relative comparisons of the fields.

IROS from the 80 mm projectile shows an enhanced quadrupolar-type residual, compared to the full shell: the residual is approximately 20% of the total field of the IROS, whereas it is approximately 10% of the main field of the full shell, at .5 normalized depths (figure 10). Note that the main field amplitude is larger for the small scrap piece than the full UXO, in the top row of figure 10, as a consequence of the absolute depth difference. At 3.0 normalized depths, the residuals are about 1% of the total field for both the IROS and the full shell; however, the residual from the IROS is still about 10 times that of the full shell (figure 11). When compared at a given normalized depth, over the range of from .5 to 3.0 normalized depths, the quadrupolar-type residuals from the full 80 mm projectile and the IROS (from its body) indicate that the scrap shows a quadrupolar-type anomaly that is about 10 times stronger than the full shell and that the anomalies from the scrap and the full shell differ significantly in spatial-spectral content. In contrast, at approximately equal absolute depths (35.7 cm, or 3 body lengths, for the scrap versus 38.7 cm: figure 11, bottom-left, or .5 body lengths, for the full shell: figure 10, bottom-right), the quadrupolar-type field of the full shell is about 150 times stronger while the anomalies have spatial spectral contents that are similar but differ in signature. At this depth the quadrupolar-type field from the IROS may be undetectable in field data, whereas the same field from the UXO remains detectable.

Differences between the tested IROS and UXO extend to the 155 mm projectile as well. The scrap model for this target is a substantial portion of the complete shell body yet it does exhibit substantial differences in quadrupolar-type anomaly, compared to the full shell, over the entire range of normalized depths. Examples appear in figures 12 and 13. The 155 scrap shows an enhanced quadrupolar type residual, compared to the full shell: the residual is approximately 27% of the main field of the scrap, whereas it is approximately 16% of the main field of the full shell, at .5 normalized depth (figure 12). At 3 normalized depths, the residual fields are about 3% and 1% of the primary field, for the scrap and full shell, respectively (figure 13). When compared at a given normalized depth, the fields from the full 155 mm projectile and the scrap (from its body) indicate that the quadrupolar-type anomaly from the scrap is about 3 times stronger than the full shell and, the anomalies from the scrap and the full shell differ in spectral content. At equal absolute depths (303 cm, or .5 body lengths of the 155 shell), the quadrupolar-type residual field of the scrap would still be about 1.4 times as large as that of the full shell, assuming an r^{-4} decay. Spatial-spectral contents also differ: the quadrupolar-type residuals at .5 normalized depths (figure 12) are a good indication of this as the body dimensions of the scrap and the full shell are quite similar in this case.

It is important to note that a prior effort investigating the non-dipole fields of ordnance (McFee and Das, 1990) assumed the quadrupole moment of the full shell is negligible, owing to assumed axial and back to front symmetry of the model as well as model deviations attributed to other sources, such as remanent magnetization, or both. Our results show that for the two modeled UXO this is not the case: the quadrupolar-type residual comprises about 10% of the total field of the 80-mm projectile and about 16% of the total field of the 155-mm projectile, at .5 body lengths. These tests include only induced moments but differ from previous modeling results in the inclusion of full geometric complexity of the shell. It is clear that inclusion of this complexity is integral

to correctly assessing the resulting fields at up to 3 normalized depths. In fact, it is exactly this complexity that accounts for the higher order quadrupolar-type residual anomaly, which we have shown to be a potentially powerful discriminator between scrap and UXO, and a robust feature of the fields within the range of 3 normalized depths (see below).

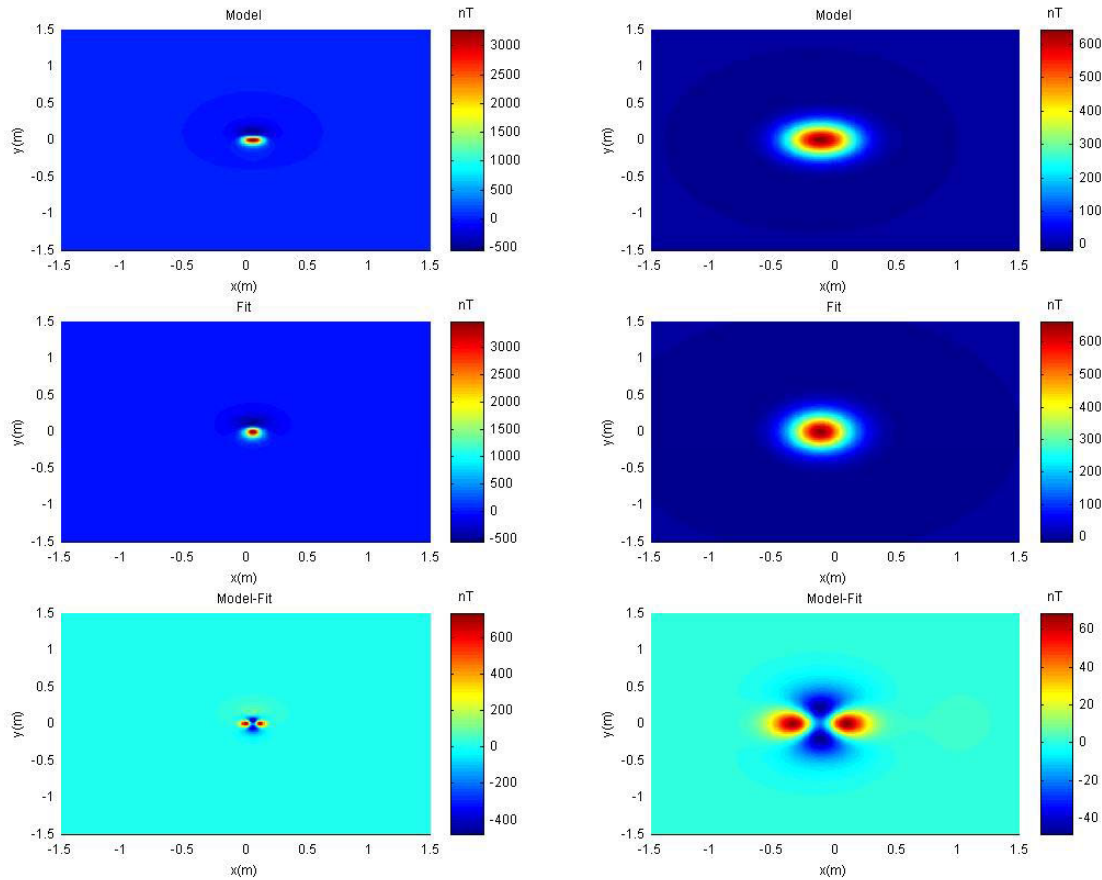


Figure 10. Fields from the 80 mm irregular scrap are shown in the left column: fields from the full 80 mm shell are shown in the right column. Each column shows vertically from the top: model data, fit to the model, and the residual of the difference. These are shown over a 1cm-sampling grid with no noise, and at a normalized depth of 0.5. The residuals differ in spatial spectrum, absolute strength, and relative strength (when compared to the respective full field). The scrap produces a quadrupolar-type residual that is more compact spatially than the UXO, is about 10 times stronger than the full UXO, and is about twice as large as the UXO field, in comparison to the total field.

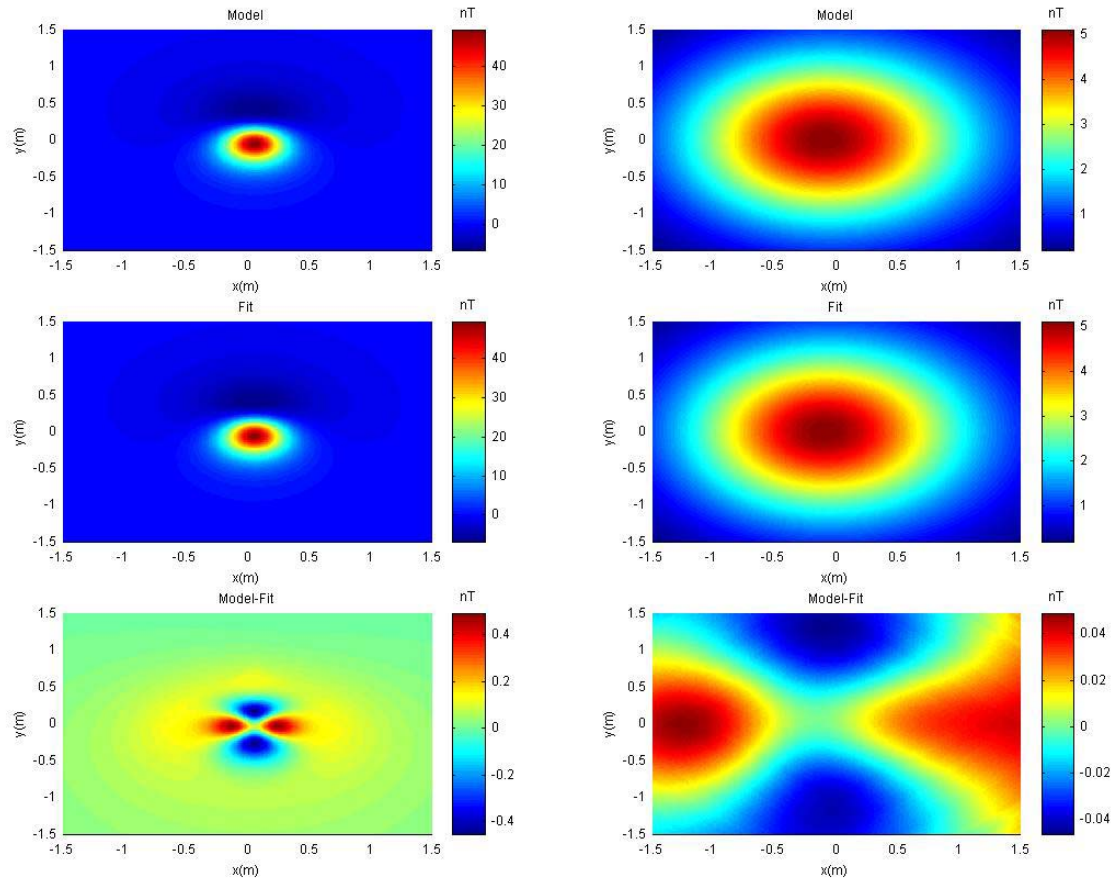


Figure 11. Fields from the 80 mm irregular scrap are shown in the left column: fields from the full 80 mm shell are shown in the right column. Each column shows vertically from the top: model data, fit to the model, and the residual of the difference. These are shown over a 1cm-sampling grid with no noise, and at a normalized depth of 3.0. The residuals differ in spatial spectrum, absolute strength, and relative strength (when compared to the respective full field). The scrap produces a quadrupolar-type residual that is more compact spatially than the UXO, is about 10 times stronger than the full UXO, and is about twice as large as the UXO field, in comparison to the total field.

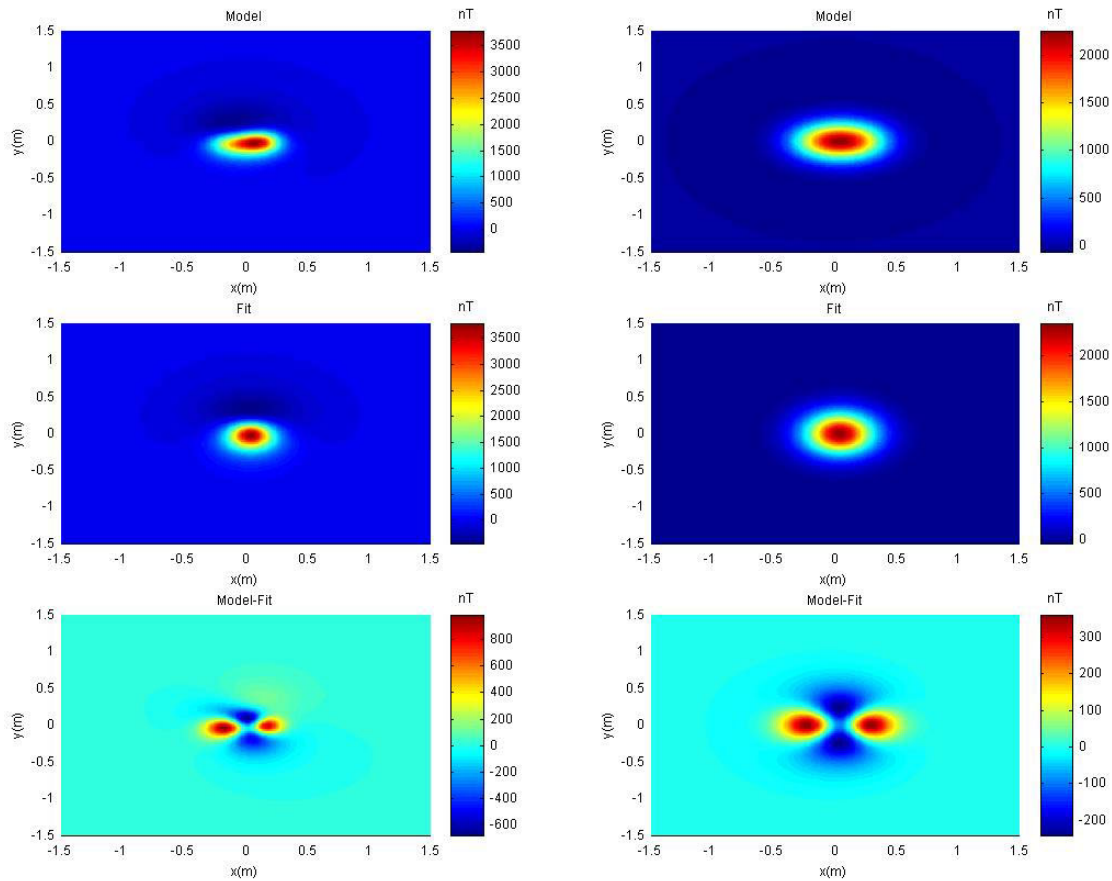


Figure 12. Fields from the 155 mm irregular scrap are shown in the left column: fields from the full 155 mm shell are shown in the right column. Each column shows vertically from the top: model data, fit to the model, and the residual of the difference. These are shown over a 1cm-sampling grid with no noise, and at a normalized depth of 0.5. The residuals differ in spatial spectrum, absolute strength, and relative strength (when compared to the respective full field).

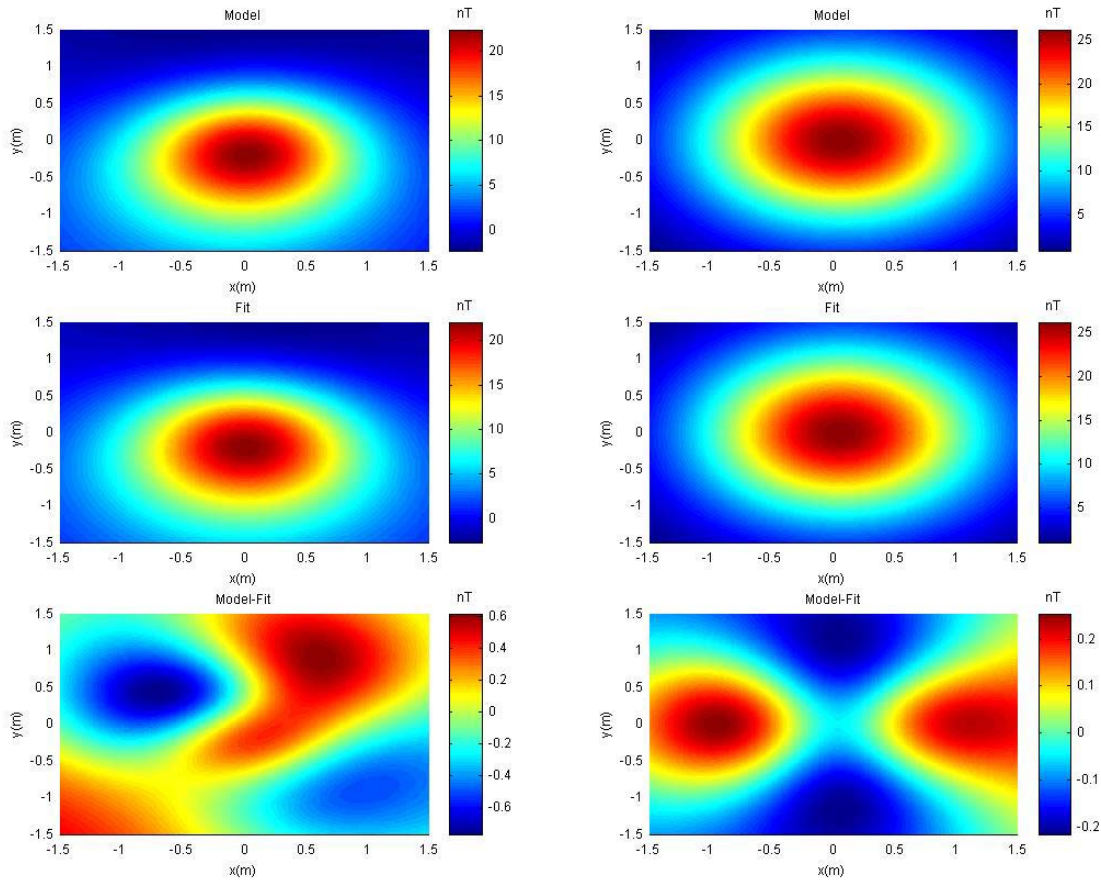


Figure 13. Fields from the 155 mm irregular scrap are shown in the left column: fields from the full 155 mm shell are shown in the right column. Each column shows vertically from the top: model data, fit to the model, and the residual of the difference. These are shown over a 1cm-sampling grid with no noise, and at a normalized depth of 3.0. The residuals differ in spatial spectrum, absolute strength, and relative strength (when compared to the respective full field) though the differences are diminished compared to shallower normalized depths.

6.3.2 Field Decay

Prolate-spheroidal-dipole fits to the fields showed residuals of quadrupolar appearance. Further evaluation of the quadrupolar-type nature of the residuals was accomplished by plotting the decay versus depth. Results for the 80-mm IROS are shown in (figure 14). The plot indicates that decay with depth is well approximated by an exponent of -4 , as would be expected for the quadrupole. Results for the other 3 items are similar, and support a quadrupolar-type residual for each item.

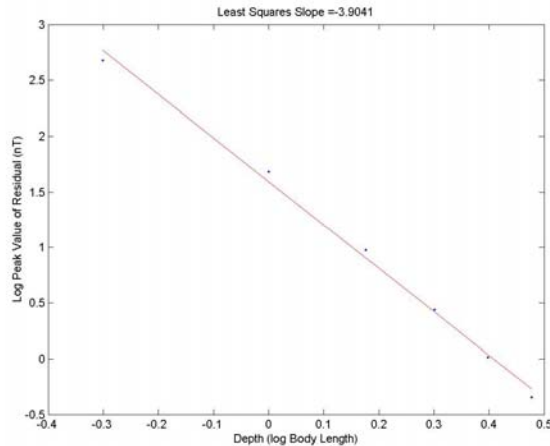


Figure 14. An initial evaluation of dipole model-fit residuals indicates that they are well approximated by decay having an exponent of -4 , as would be expected for a quadrupole: the log-log plot above shows a least squares fit to the slope of approximately -3.9 . Hence, residuals from IROS modeled from the 80-mm projectile not only appear quadrupolar but also decay as quadrupoles.

6.4 Noisy Data Inversion Residuals

The effects of sensor noise and positioning errors on the quadrupolar-type residual fields were tested in a sensitivity analysis. Evaluation of the effects of sensor noise and positioning errors proceeded from independent evaluation, over a range of values spanning those expected in the field, to combined testing. The results are discussed below.

6.4.1 Sensor Noise

Gaussian-noise with standard deviations of 0, .25, and 1.25 nT was added to the modeled data, sampled at 5 cm over 3x3 m grids, to simulate additive sensor noise. This resulted in 3 different noisy forward models for each target, at each of 6 different normalized depths (.5 to 3.0 in increments of .5). A total of 72 different noisy models were calculated and fit.

The results showed that sensitivity to the noise increased as the normalized depths increased, as expected. Noise with a 1 nT standard deviation was not sufficient, even at 3 normalized depths, to prevent a good fit to the 80 mm scrap data. An example of the residual from a normalized depth of 2.0 is shown in figure 15. In contrast, when the noise standard deviation is 5 nT, the quadrupolar-type residual anomaly cannot be seen past 1.5 normalized depths, without filtering. An example from a normalized depth of 2.0 is shown in figure 16. Although it is beyond the present scope, SIV found it important to evaluate the possibility of recovering the quadrupolar-type signature when the data are contaminated by noise. The residual of figure 16 can be seen in figure 17 before (a) and after (b) low-pass filtering. The quadrupolar-type residual can be seen after filtering at 2.0 normalized depths. Beyond this depth, the residual is not recoverable using simple filtering. Equivalent results were obtained with the scrap from the 155 mm.

6.4.2 Positioning Noise

Gaussian positioning errors with equal standard deviations of .5, 1, and 2 cm, along the x and y principal axes were added to the measurements to simulate additive navigation noise. These errors degrade the visual expression of the residual signature to a much greater extent than do the amplitude variations (figures 18 and 19). Irregular sampling, imposed by the navigation errors, requires re-gridding for visual display, as in figure 19a. The visual appearance of the residual anomaly, even at .5 cm standard deviation, is essentially completely destroyed. Filtering, however, is able to recover the quadrupolar-type residual (figure 19b). Similarly, at a noise standard deviation of 1 cm, the quadrupolar-type residual is recoverable, after filtering out to 2.5 normalized depths (figure 20): in field application this signal is close to the practical noise floor of common sensors. At a noise standard deviation of 2 cm, consistent with the maximum accuracy of an RTK GPS, the quadrupole-type anomaly from the 80-mm scrap cannot be detected at any of the normalized depths tested, even after filtering (figure 21 shows this for 2.5 normalized depths for comparison with prior figures). In contrast, the 155 scrap can be distinguished without filtering at .5 normalized depths, and can be distinguished after filtering to at least 1.5 normalized depths, even with a noise standard deviation of 4 cm (figure 22a and b).

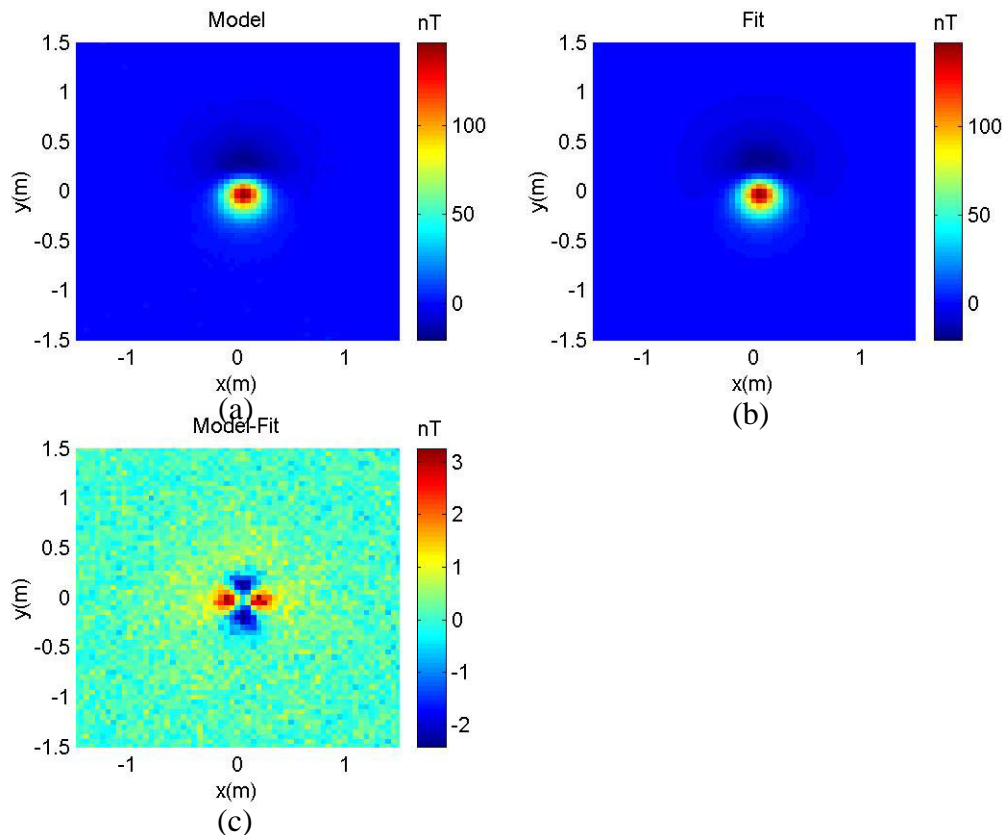


Figure 15. The field from the irregular scrap of the 80-mm, in a vertical 60,000 nT earth field, at 2.0 normalized depths, 5 cm sampling, and with additive Gaussian noise of 1 nT standard deviation: (a) total field; (b) fit; (c) quadrupolar-type residual. Sensor noise of 1 nT standard deviation results in a residual that can still be discerned at a normalized depth of 2, and with a sample spacing of 5 cm.

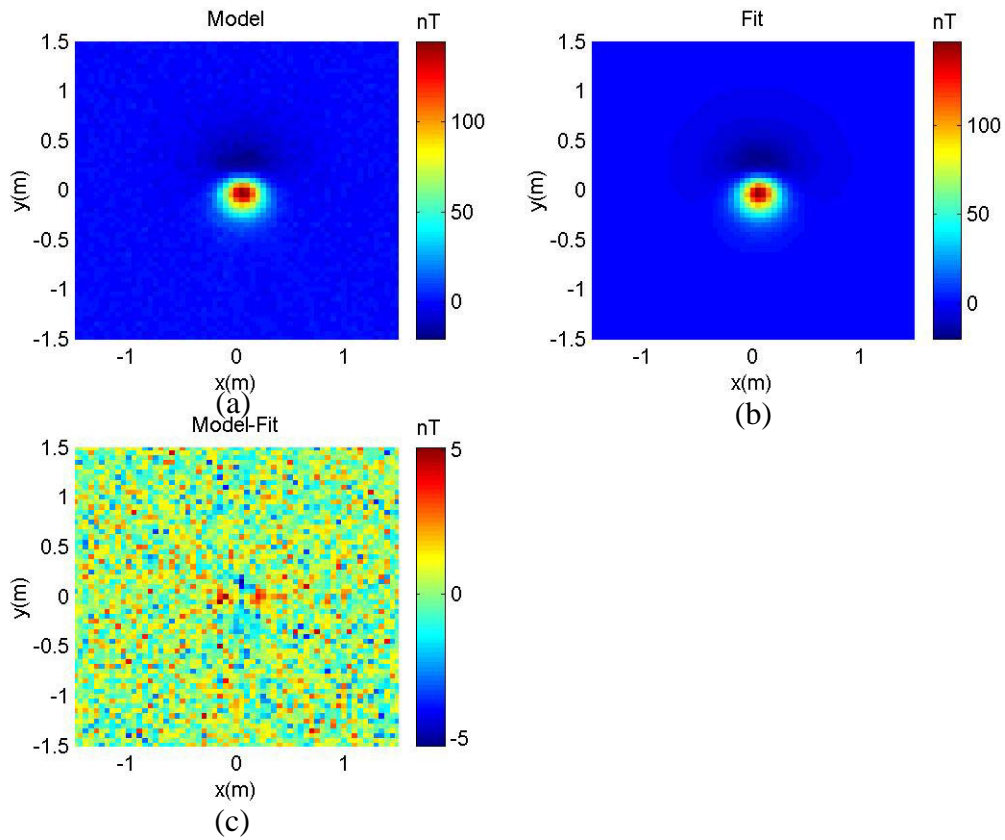


Figure 16. Field from the irregular scrap of the 80-mm, in a vertical 60,000 nT earth field, at 2.0 normalized depths, 5 cm sampling, and with additive Gaussian noise of 5 nT standard deviation: (a) total field; (b) fit; (c) quadrupolar-type residual. Amplitude noise of 5 nT standard deviation results in a residual that cannot be discerned at a normalized depth of 2.0, and with a sample spacing of 5 cm.

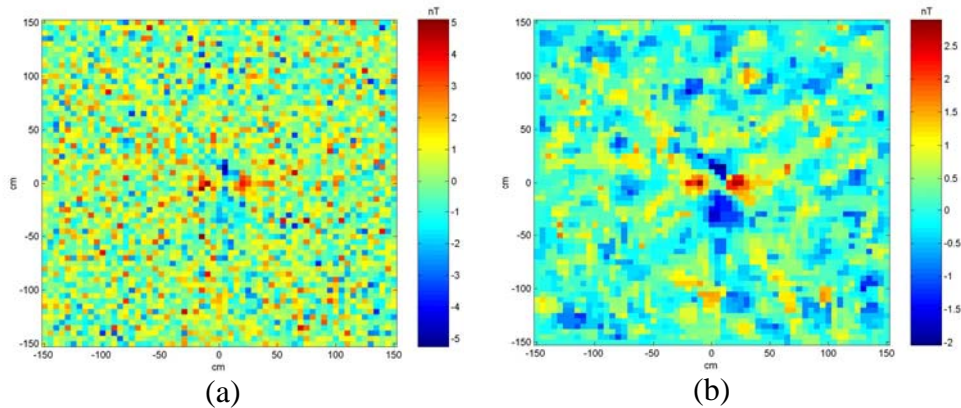


Figure 17. Comparison of the residual field from figure 16 with the residual field after filtering: despite an SNR of about -10 dB, the quadrupolar-type anomaly is still detectable after filtering, at a normalized depth of 2.0, and with a sample spacing of 5 cm.

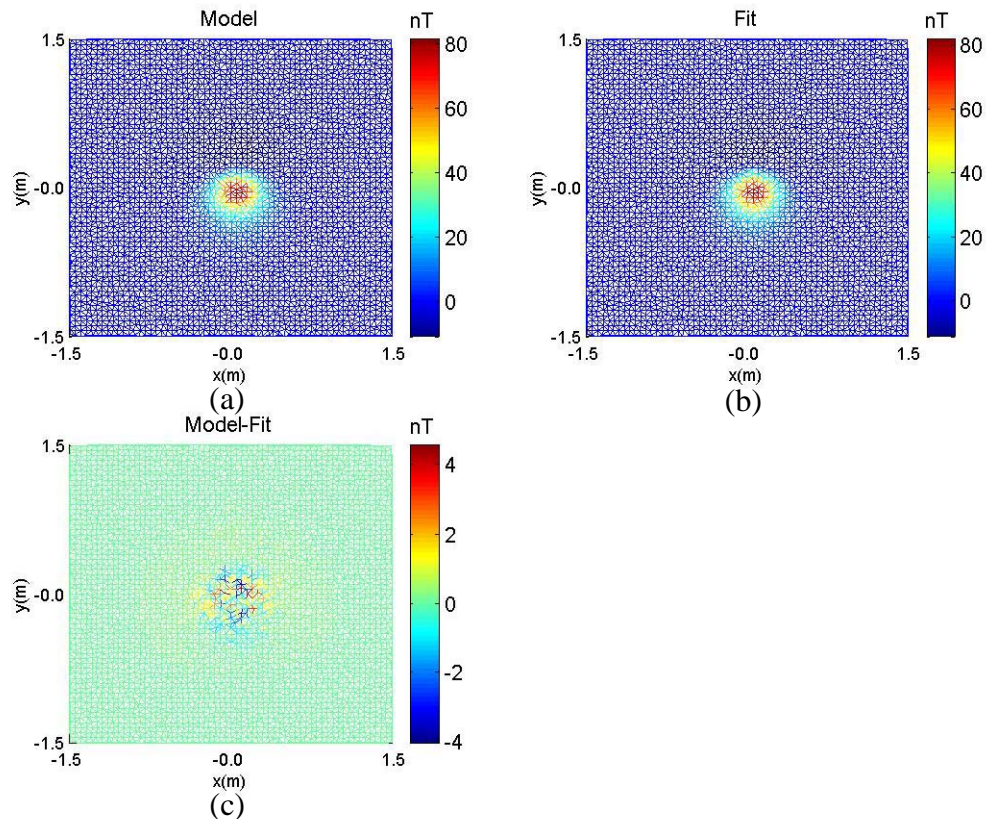


Figure 18. Field from the IROS of the 80-mm, in a vertical 60,000 nT earth field, at 2.5 normalized depths, 5 cm intended sampling, and with additive Gaussian positioning noise of .5 cm standard deviation: (a) total field after adding the noise; (b) fit; (c) quadrupolar-type residual. Positioning errors introduce an irregularly sampled grid, which cannot be directly compared to the original regularly sampled grid: these data are not very informative unless they are gridded, as can be seen above. The following figures show the gridded residuals to enhance the visual display.

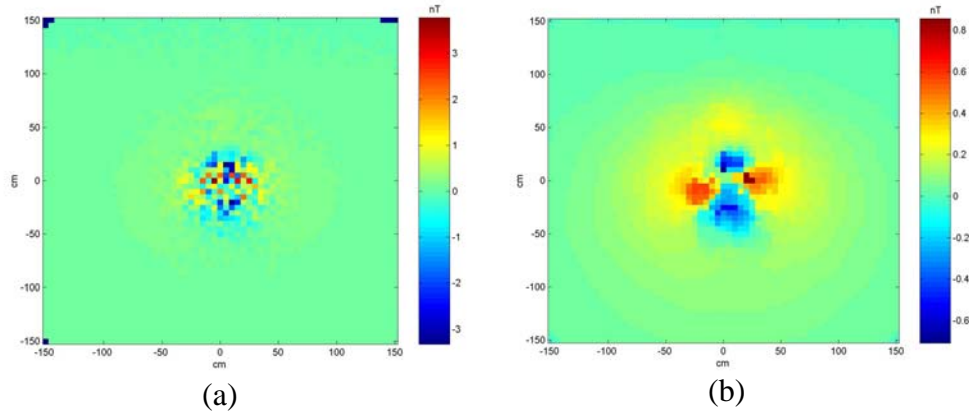


Figure 19. Same as in figure 18 but (a) with gridded residual; (b) after filtering, the quadrupolar-type anomaly can be discerned.

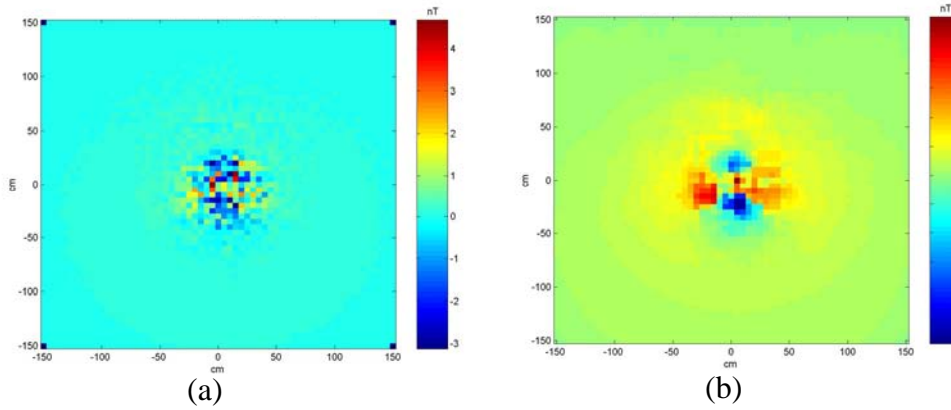


Figure 20. Same as in figure 18 but (a) gridded residual with navigation noise increased to 1 cm standard deviation; (b) after filtering, the quadrupolar-type anomaly can be discerned.

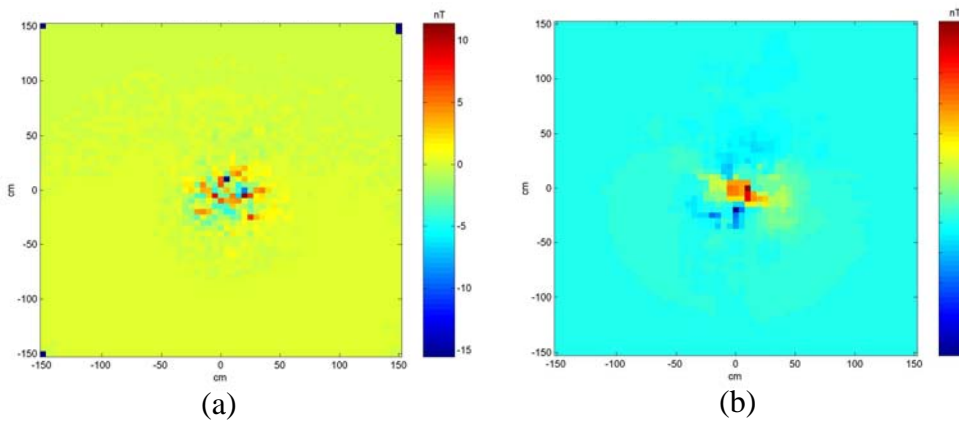


Figure 21. Same as in figure 18 but (a) gridded residual with navigation noise increased to 2 cm standard deviation; (b) after filtering, the quadrupolar-type anomaly still cannot be discerned.

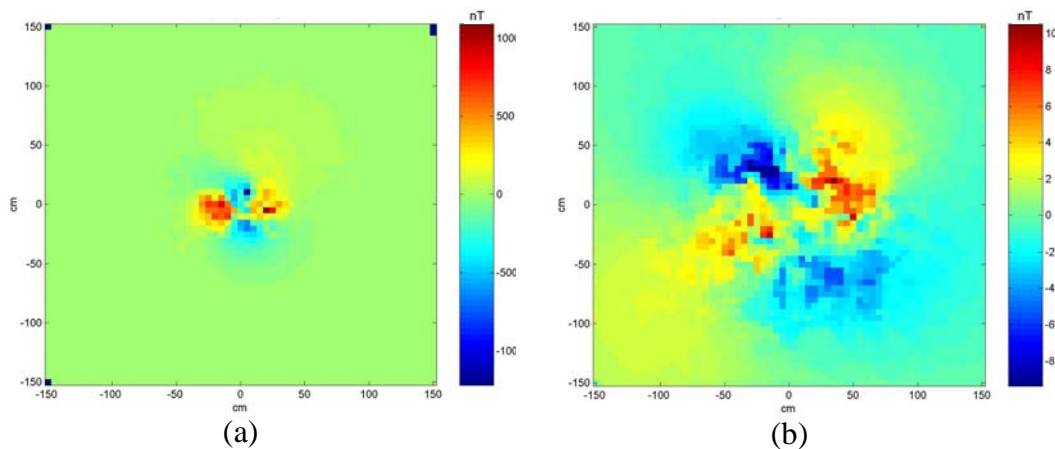


Figure 22. Gridded residual fields from the 155 mm IROS, in a vertical 60,000 nT earth field, 5 cm intended sampling, and with additive Gaussian positioning noise of 4 cm standard deviation: (a) unfiltered at .5 normalized depths, the quadrupolar field is discernible; (b) at 1.5 normalized depths, after filtering, the quadrupolar-type anomaly can still be discerned: it may be detectable to 3 normalized depths, depending upon the filtering applied.

6.4.3 Sensor and Positioning Noise

The noise ranges from the above tests, on individual parameters, were tested in combination to evaluate the degradation that might be expected in real data subjected to both additive sensor and positioning errors as the primary noise sources. Although not within the present scope of work, SIV found it important to demonstrate that despite the apparent destruction of the quadrupole, as a result of sensor and/or positioning noise, the signature can be recovered by filtering the input data. This demonstrates the robustness of the signature to realistic noise fluctuations.

Results of these tests indicate that at a standard deviation of 4 cm navigation noise and a 5 nT standard deviation amplitude noise permits detection of the 155 mm IROS to 1.5 normalized depths (figure 23), but not below, even after simple filtering. As described above, the quadrupolar-type residual from the 80 mm IROS cannot be seen, even after filtering, at any depth for navigation noise of 2 cm standard deviation. When the navigation noise is reduced to 1 cm with a 5 nT standard deviation amplitude noise, detection of the quadrupolar-type residual from the 80 mm scrap to 1.5 normalized depths is seen (figure 24), but not below, even after filtering. If, however, the standard deviation of sensor-noise is diminished to 1 nT, the quadrupolar-type residual is detectable after filtering to 2.5 normalized depths (figure 25).

Interaction of one or more noise sources with the non-dipole field of an item is a complex process as the fields must be derived indirectly from the measurements and noise may contaminate this initial step. We have investigated some specific practical cases in an attempt to provide insight into real field performance and this has demonstrated that despite the complexity, the non-dipole signatures investigated are robust to typical noise sources over a range of depths of interest.

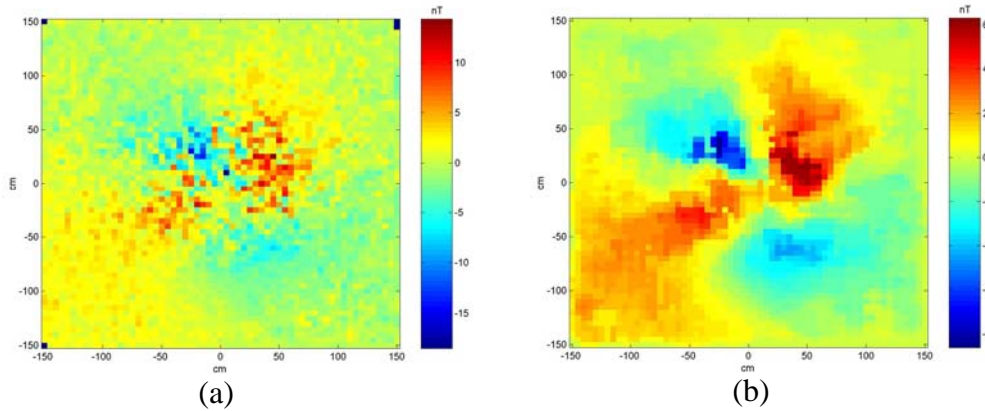


Figure 23. Gridded residual (a) with navigation noise of 4 cm standard deviation, amplitude noise of 5 nT standard deviation (SNR of about -6dB from amplitude noise alone), and at a normalized depth of 1.5, for IROS from a 155 mm; (b) after filtering, the quadrupolar-type anomaly can be discerned.

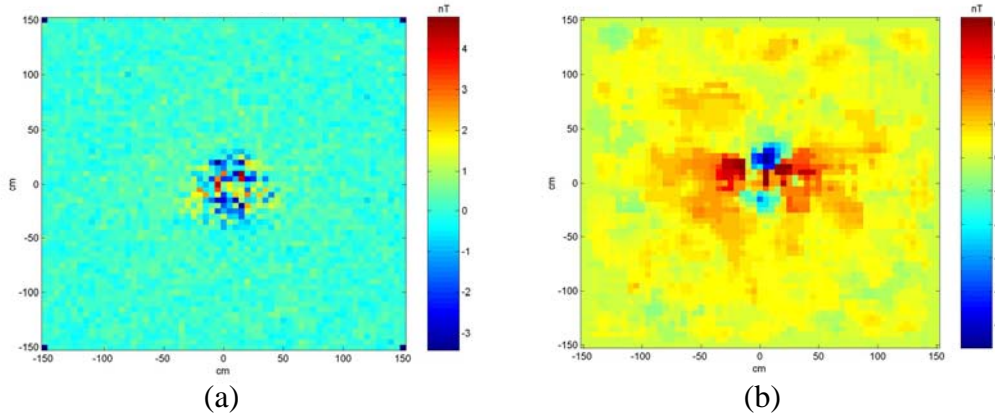


Figure 24. Gridded residual (a) with amplitude noise of 1 nT standard deviation, navigation noise of 1 cm standard deviation, and at a normalized depth of 2.5; (b) after filtering, the quadrupolar-type anomaly can be discerned.

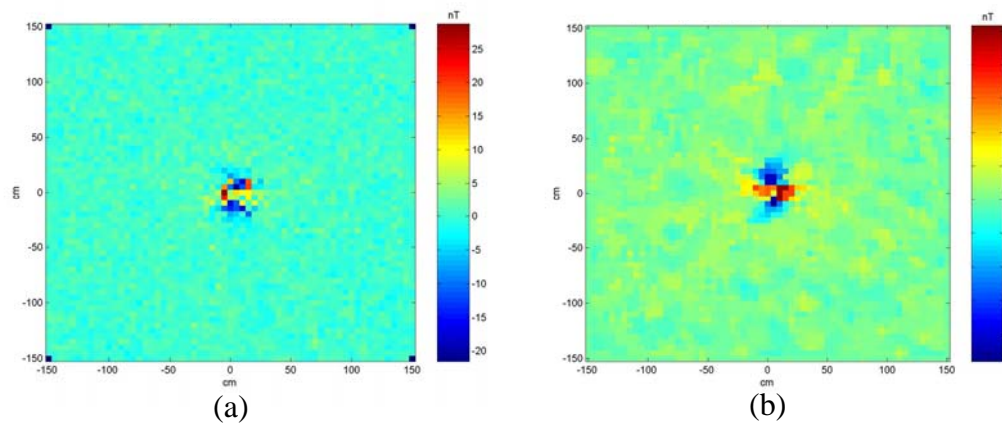


Figure 25. Gridded residual (a) with amplitude noise of 5 nT standard deviation, navigation noise of 1 cm standard deviation, and at a normalized depth of 1.5; (b) after filtering, the quadrupolar-type anomaly can be discerned.

6.5 Sampling

Quadrupolar-type residuals have shorter spatial wavelengths than their associated full field anomalies. As a result, sampling requirements for these fields are more stringent than those required for the full-field anomalies. The depth dependent non-dipole signatures, obtained from subtraction of the inverted dipole fields, provide the basis for evaluation of the effects of sampling density on the spatial signatures and consideration of field-data collection requirements. Testing of model data sampled at different practical sampling densities revealed a tradeoff between sampling density, collection time and effort, and loss of information. These tests were supplemented by an evaluation of window effects and spectral evaluation of the smallest target (80-mm IROS), at the shallowest depth, and highest density sampling. This provided more precise sampling criteria to recover the quadrupolar-type signature of this target, and others like it.

6.5.1 Sampling Density

Sampling densities were varied from 1 cm to 5 cm and 10 cm for the 80-mm IROS (11.9 cm long) and to 20 cm for the 155-mm IROS (50.0 cm long). For the 80 mm IROS, sampling at 1 cm shows a high fidelity residual at all normalized depths investigated (.5 to 3 in increments of .5). At 5 cm sampling, the quadrupolar-type residual appears aliased at the shallowest normalized depth (.5, figures 26 and 27) and is reproduced at all other investigated depths. At 10 cm sampling interval, the quadrupolar-type residual is aliased below a normalized depth of 2.0 (figures 28 and 29). The quadrupolar-type residual from the intact projectile is reproduced at all normalized depths, even at 10 cm sampling (figure 30).

In contrast, the quadrupolar-type residual from the 155 scrap is reproduced at all depths using a 5 cm or a 10 cm sampling (figure 31). At 20 cm sampling, the quadrupolar-type residuals below 1.5 normalized depths appear aliased and those above these depths appear low resolution (figure 32). At 20 cm sampling density, the differences between the 155 scrap and full 155 persist even down to 1 normalized body length (figures 8 and 9). At half a normalized body length the sampling is too coarse to discern the differences in residual. The differentiability of the targets from the quadrupolar-type residuals is detectable despite the fact that the 155 scrap represents a substantial portion of the shell body and the two targets differ only in a longitudinal “cap” that would complete the scrap shell. Additionally, we expect that this is the worst case for the full shell, as it is horizontal and we expect the quadrupolar-type residual will diminish for other orientations of the full shell. In contrast, the scrap is expected to retain significant quadrupolar-type residuals at other orientations. Therefore, we expect that discrimination between scrap and the full shell will be a robust property of the quadrupolar-type fields.

These results indicate that the practical implementation of the quadrupolar detection methodology will require a tradeoff of time (to achieve the desired sampling density) versus the quadrupolar-type anomaly detection limit (for the smallest target of interest, and at the shallowest depth of interest), considering the possible range of target anomaly sizes and depths. It is important to note that the sampling requirements for unaliased non-dipole fields of even the largest intact UXO (155-mm here) are not generally

achieved in standard surveys and even existing “high resolution” surveys may only be capable of recovering low resolution images of the non-dipole fields.

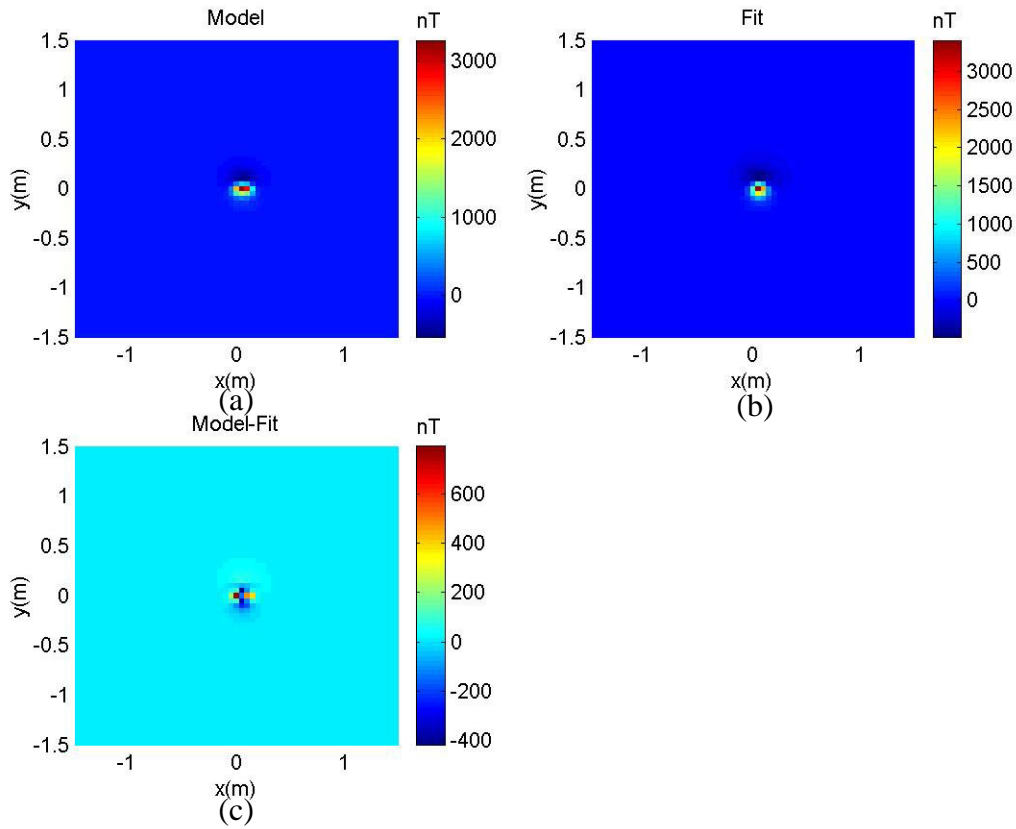


Figure 26. The fields from the 80-mm IROS, at 0.5 normalized depths and 5 cm sample spacing: (a) forward model; (b) fit; and (c) the residual shows an aliased quadrupolar-type residual.

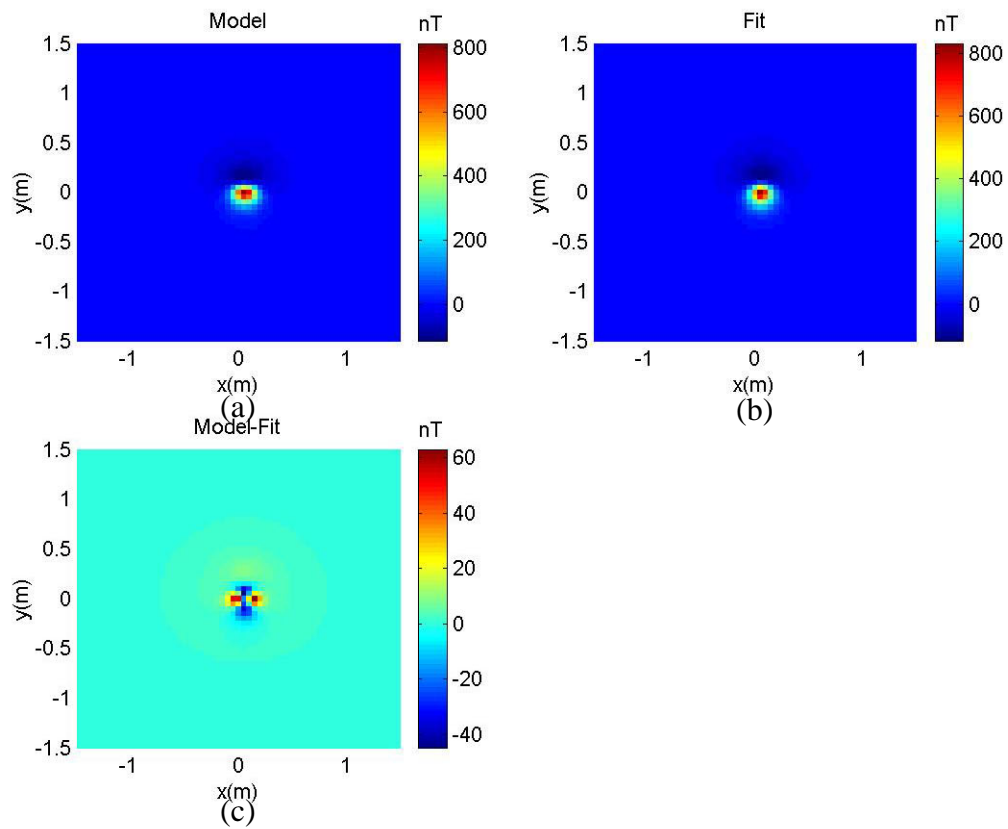


Figure 27. The fields from the 80-mm IROS, at 1.0 normalized depths and 5 cm sample spacing: (a) forward model; (b) fit; and (c) the residual shows an unaliased quadrupolar-type residual.

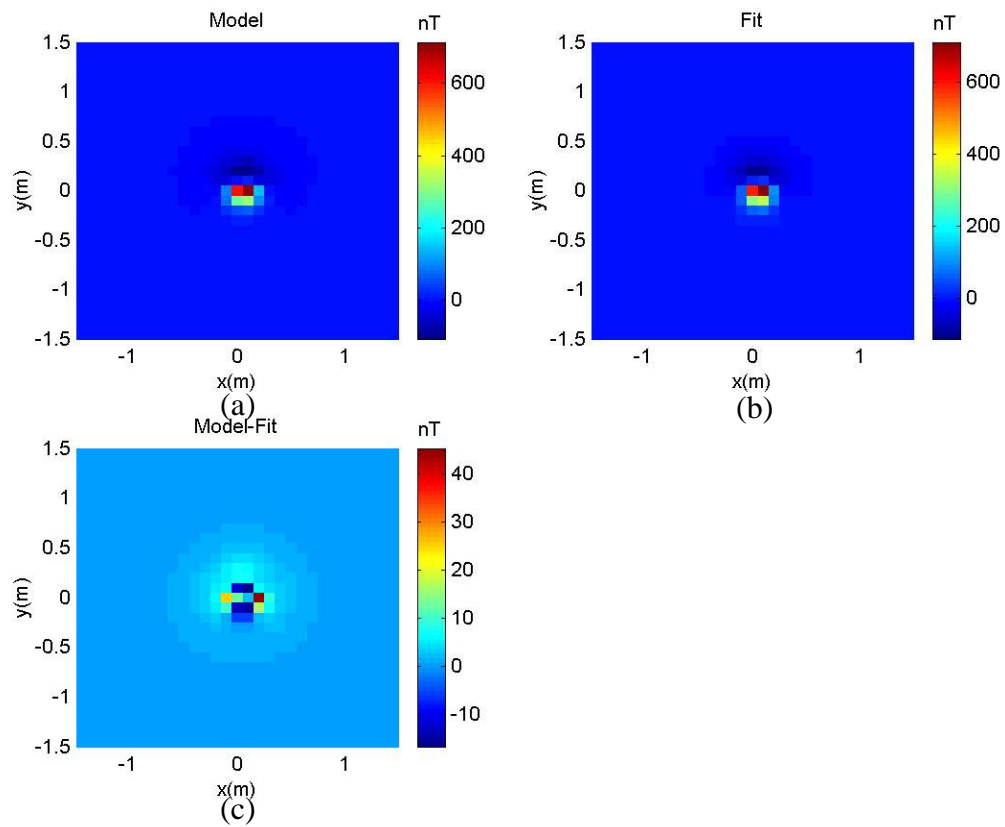


Figure 28. The fields from the 80-mm IROS, at 1.0 normalized depth and 10 cm sample spacing: (a) forward model; (b) fit; and (c) the residual shows an aliased quadrupolar-type residual.

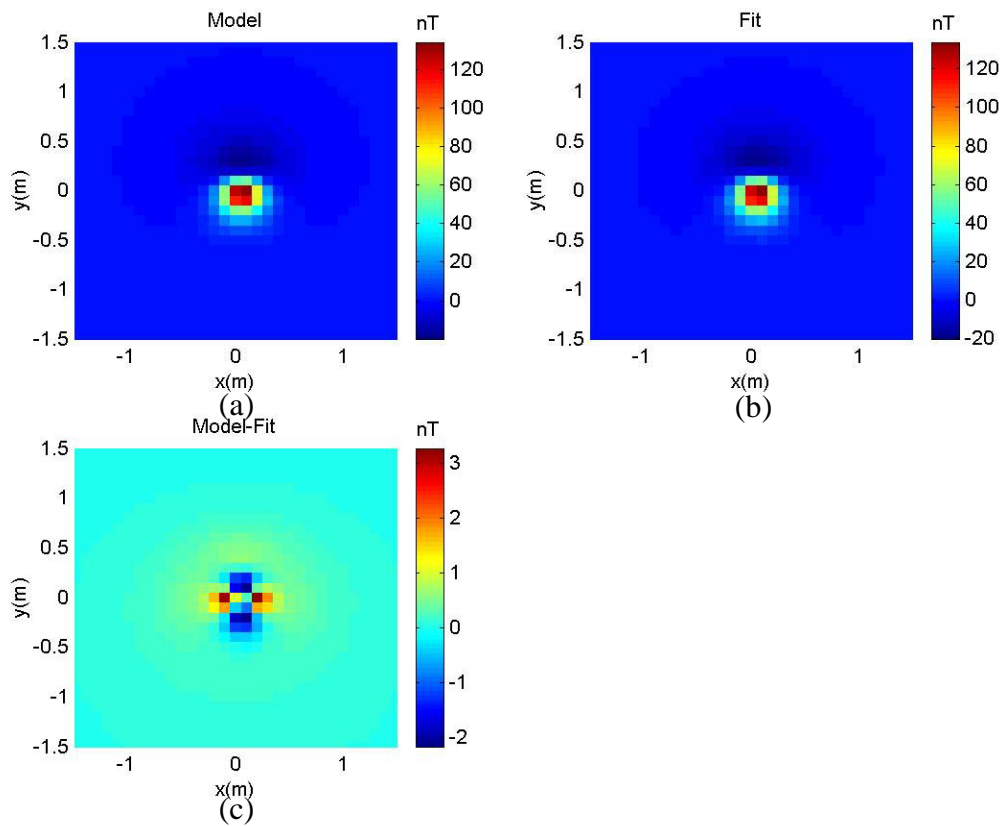


Figure 29. The fields from the 80-mm IROS, at 2.0 normalized depths and 10 cm sample spacing: (a) forward model; (b) fit; and (c) the residual shows an unaliased quadrupolar-type residual.

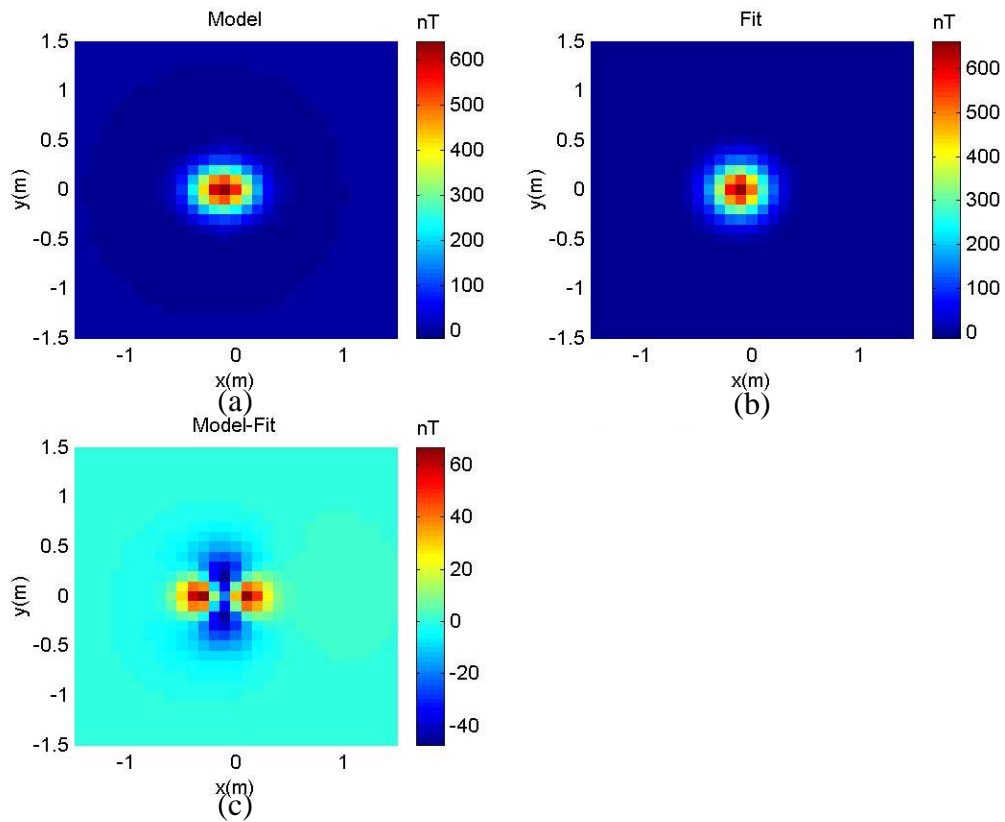


Figure 30. The fields from the intact 80-mm projectile, at 0.5 normalized depths and 10 cm sample spacing: (a) forward model; (b) fit; and (c) the residual shows an unaliased quadrupolar-type residual.

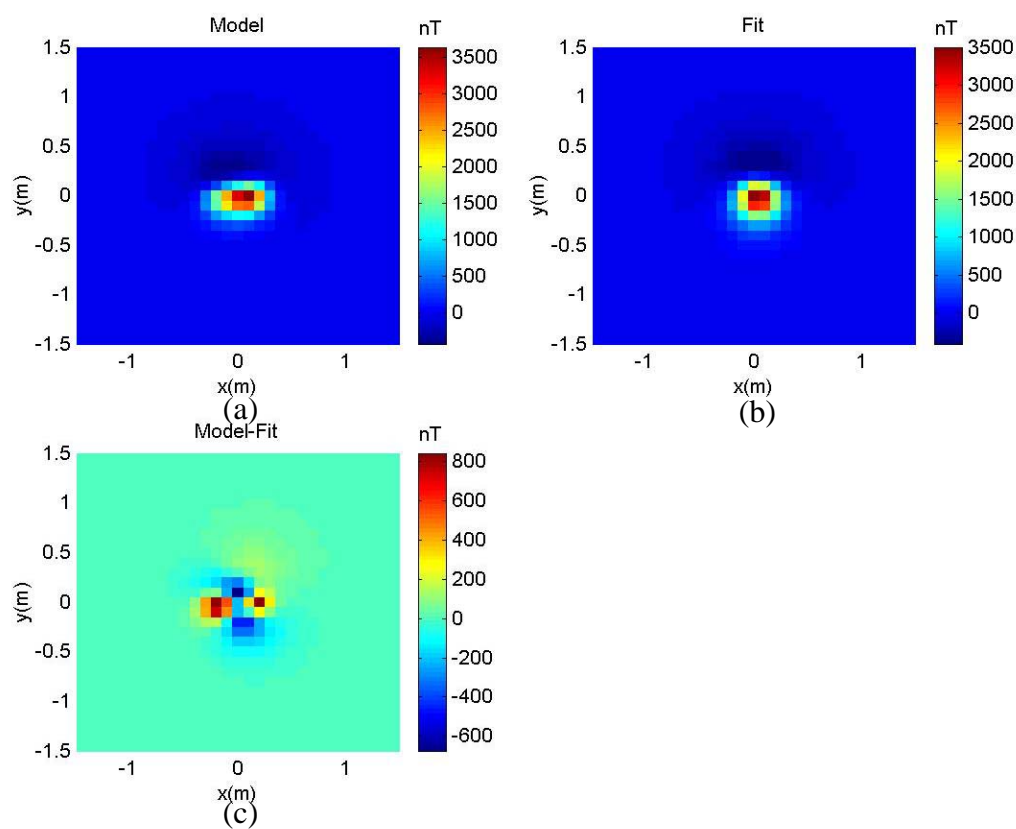


Figure 31. The fields from the 155-mm IROS, at 0.5 normalized depths and 10 cm sample spacing: (a) forward model; (b) fit; and (c) the residual shows an unaliased, albeit low resolution, quadrupolar-type residual.

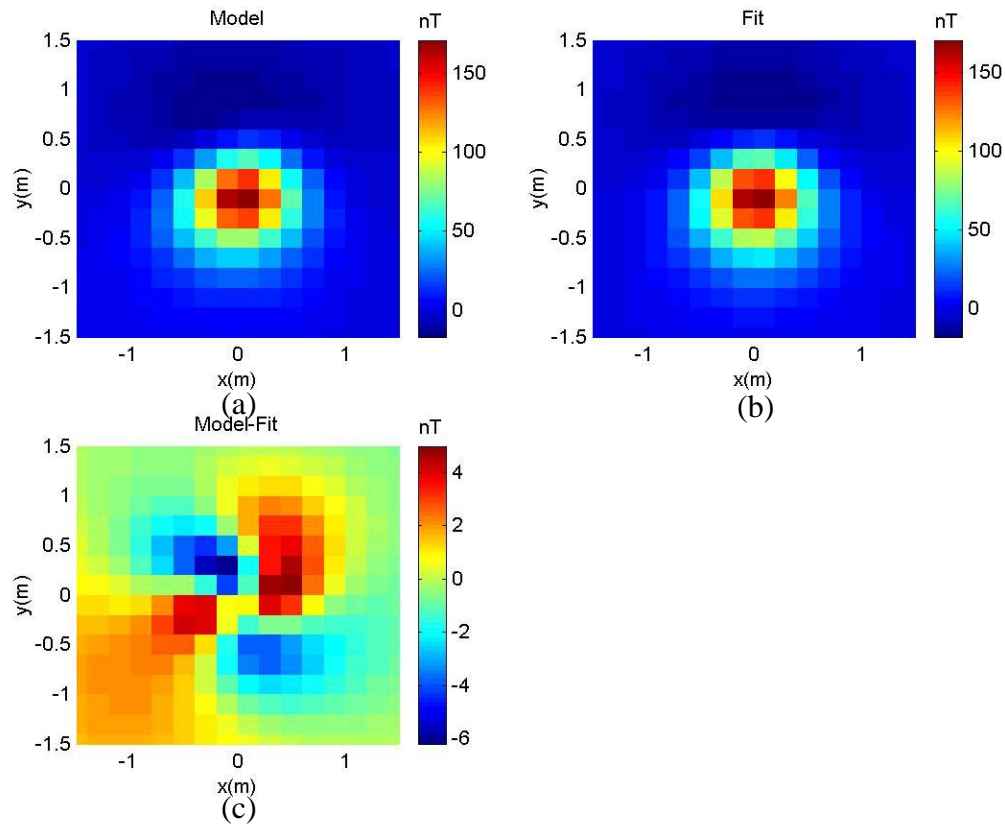


Figure 32. The fields from the 155-mm IROS at 1.5 normalized depths and 20 cm sample spacing: (a) forward model; (b) fit; and (c) the residual shows an unaliased, albeit low resolution, quadrupolar-type residual at depths equal to or greater than this depth.

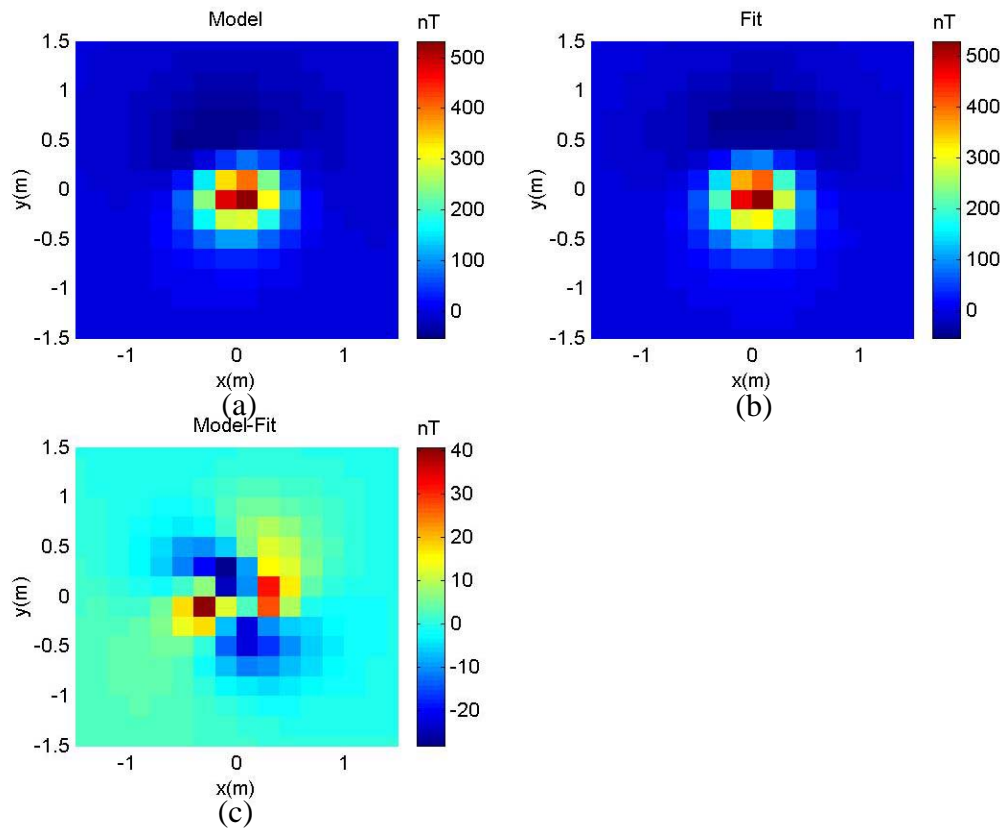


Figure 33. The fields from the 155-mm IROS at 1.0 normalized depths and 20 cm sample spacing: (a) forward model; (b) fit; and (c) the residual shows an unaliased, albeit low resolution, quadrupolar-type residual that differs from that of the full shell (figure 34).

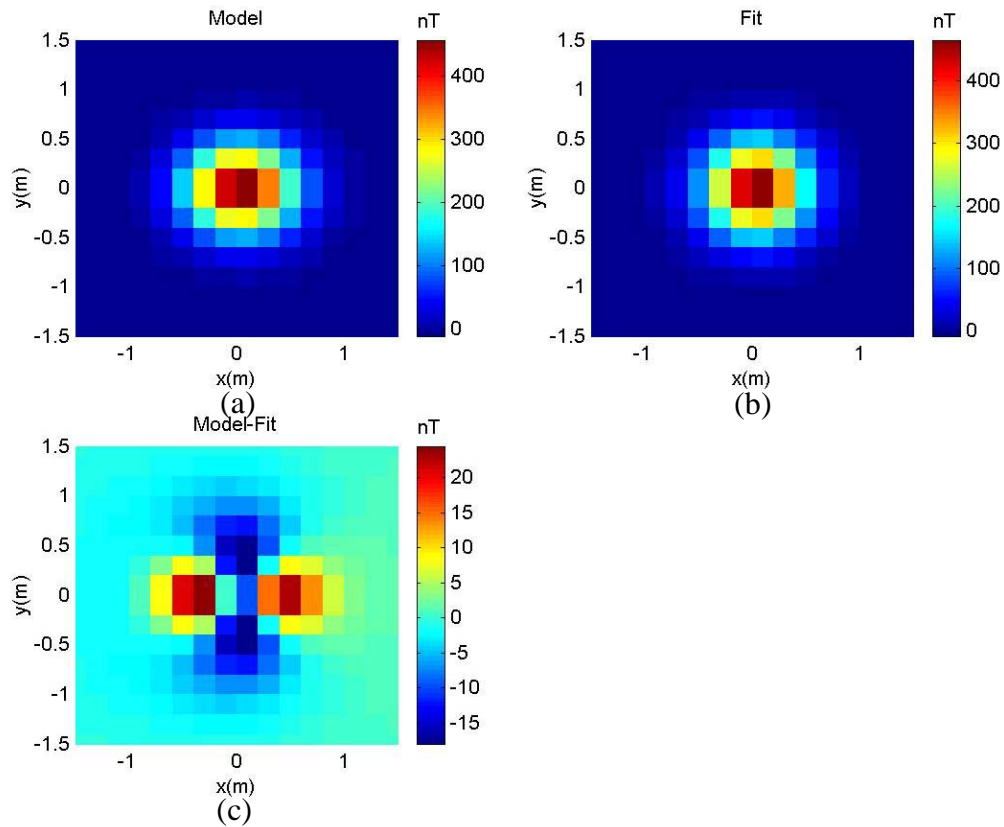


Figure 34. The fields from the 155-mm, intact, projectile at 1.0 normalized depths and 20 cm sample spacing: (a) forward model; (b) fit; and (c) the residual shows an unaliased, albeit low resolution, quadrupolar-type residual that differs from that of the scrap (figure 33).

6.5.2 Sampling Window

A constant sampling window of 3x3m was used in all the results shown above. This window has no effect on the data until the 155 mm projectile, or the large scrap piece from it, is encountered at depths below 1.5 body lengths. At depths below 1.5 body lengths, despite an excellent anomaly fit and an accurate depth estimate, the quadrupolar type anomaly becomes increasingly difficult to discern due to truncation by the window (figure 35). At these depths, truncation effects may be irrelevant: our noise sensitivity analysis showed that the quadrupolar residual is on the order of the expected noise and may remain buried in the noise below 2 normalized depths, even after simple filtering. Prior knowledge of the dipole field permits data collection on a larger window, if this is deemed desirable and operationally feasible.

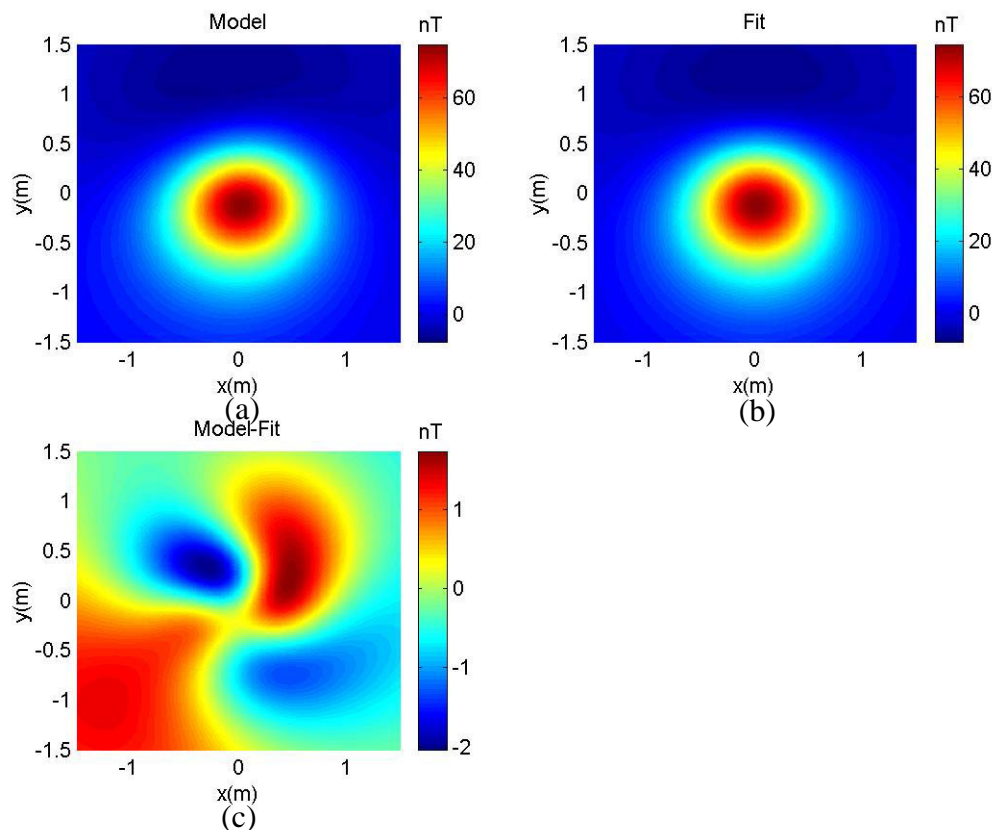


Figure 35. The fields from the 155-mm IROS at 2.0 normalized depths and 1 cm sample spacing: (a) forward model; (b) fit; and (c) the residual shows that the anomaly has started to extend beyond the window and is truncated by it. This may diminish discrimination capabilities unless the window is enlarged, assuming that the residual can be discerned above the noise.

6.5.3 Spectral Analysis

Although not within the scope of the present effort, we have evaluated the spectral signature of the quadrupolar-type residual arising from the smallest target, the 80-mm IROS (11.9 cm long) at its shallowest depth (.5 body lengths, or about 6 cm) to determine the limits of practical sampling to recover this signature. These requirements constitute the most stringent requirements for sampling: sampling at this density would be capable of recovering all targets of this size or larger. The results (

figure 36) show that the spectral power decays towards the Nyquist wavenumber, indicating that there are essentially no spectral components that have been aliased by the 1 cm sampling of the investigated grid. Based upon the spectrum, a conservative sampling would be at 1.5 cm sample spacing. We have found, however, that a sample spacing of 2.25 to 3.0 cm will still capture the most significant part of the spectrum and have no noticeable effect on the anomaly fidelity.

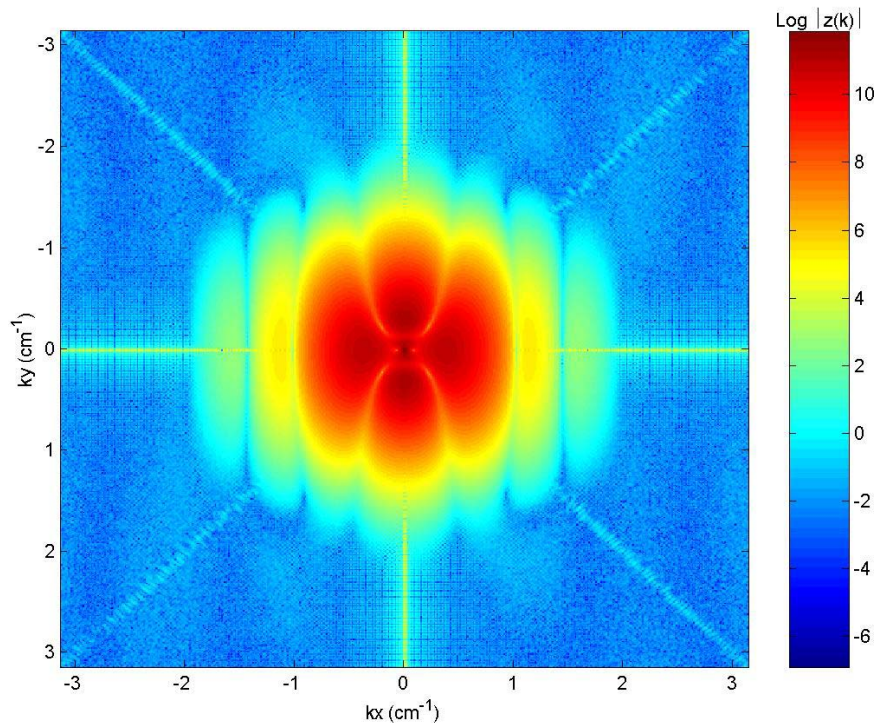


Figure 36. The spectrum of the quadrupolar-type residual from the 80-mm IROS (11.9 cm long) at its shallowest depth (.5 body lengths, or about 6 cm) and sampled in space at 1 cm.

6.6 Experimental

Data collection, for the purpose of validating the theoretical predictions, was undertaken using two UXO and two IROS targets. The importance of positioning was identified in the theoretical work, which made it clear that a hand-held scanning sensor would not achieve the accuracy required, without an engineering effort beyond the scope of this project. As a result, the experimental effort focused on designing a nonmagnetic platform that could be used for accurately scanning the investigated targets at different elevations. Owing to site access issues, the original site was unavailable for use in a time frame that would accommodate this effort, as a result, a backup site was chosen. The backup site had a higher noise level than the original site.

6.6.1 Targets

Two UXO, a 57 mm and a 20 mm projectile, as well as two IROS, the rusted base of a 155-mm and a small portion of the nose of the same size projectile were obtained from the Aberdeen Test Center for use in our field tests. Each target appears in figure 37 in correct orientation, relative to the actual line-collection direction.



Figure 37. Measurements over each of the two UXO (57 mm and 20 mm projectiles) and 2 IROS (155 mm base and 155 mm nose section) targets were made with each target positioned at the center of the platform, “primary axis” perpendicular to the line direction (shown in red). The orientation of each item, reflects its orientation relative to the collection direction during surveying: the upper end of each item (“nose”), as shown in the figure, pointed towards increasing line number. Five planes, at varying multiples of the body-length, were collected above each target.

6.6.2 Setup

The G858 magnetometer has been selected as the sensor as we have been unable to obtain an alternative.

SIV designed a completely nonmagnetic platform with a sensor traversal mechanism and a means of adjusting sensor height (without having to move the platform) and the flexibility to move the target, if necessary. Sensor and target height adjustments eliminated potential platform re-leveling at each height and the attendant errors. An 8 foot by 4 foot platform was selected to enable detailed data collection over the set of targets, at the required density, while limiting the time to collect data. The platform can be leveled to within 1 degree in 8 feet. This translates into elevation changes of less than 1.7 inches (4.2 cm), which we consider acceptable based upon the prior theoretical results. The platform, transport mechanism, and sensor are shown in figure 38.



Figure 38. The data collection platform is completely nonmetal. It is 4'x8' and incorporates a guide to align the sensor transport mechanism along a line with an error of less than $\frac{1}{4}$ inch (.62 cm). The target under investigation is placed beneath the platform center and lines are collected along the length of the 4x8 foot surface. The combination of raising the sensor or lowering the target provides flexibility in achieving the desired heights of collection planes above each target.

6.6.3 Data Collection

Data were collected, as shown in figure 39, over each of the targets shown in figure 37. Five planes of data were collected over each target at offsets ranging from 0.5 to 3.0 body lengths. A tabular representation of the targets and the 20 planes of data collected appears in table 1.

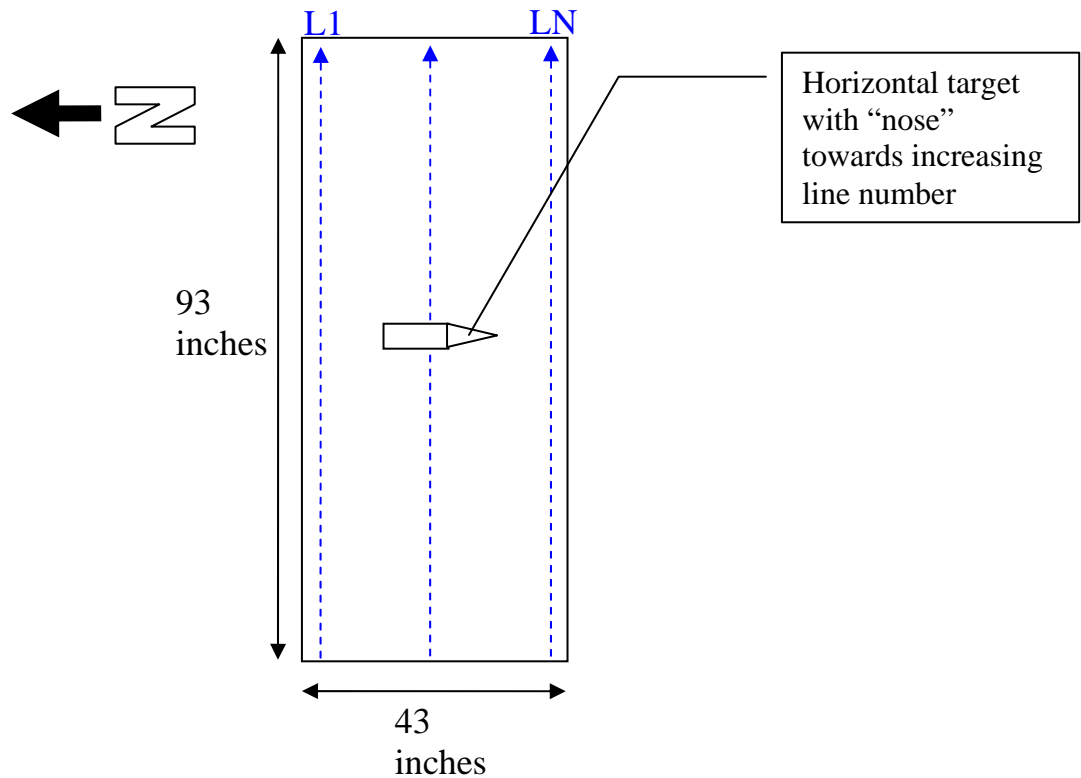


Figure 39. Experimental geometry includes 43 lines, each 93 inches long: they are asymmetric about the center at line 20, with the first line being collected from the lower left to the upper left along the length of the platform. The larger offsets enhance the anomalies in the higher planes, over the larger targets. Each target was placed below the center of the platform, perpendicular to the line direction, and with its "nose" pointing towards increasing line number.

Table 1. Data collection planes. The planes are designated in body lengths (L) with actual heights listed for each target. The five gray-filled heights appearing next to each target were collected, very small and very large offsets being eliminated.

Item	L/2	Body Length (L in inches)	3L/2	2L	5L/2	3L
Small Scrap	1 25/32	3 9/16	5 11/32	7 1/8	8 29/32	10 11/16
Large Scrap	6 9/16	13 1/8	19 11/16	26 1/4	32 13/16	39 3/8
20 mm	1 1/2	3	4 1/2	6	7 1/2	9
57 mm	3 3/8	6 3/4	10 1/8	13 1/2	16 7/8	20 1/4

6.6.4 Data Inversion Residuals

Collected target data were evaluated for quadrupolar-type residuals. Representative results appear in figures 40-45. Despite horizontal artifacts, caused by inaccurate linear positioning, the original anomalies of the larger IROS and the 57 mm, measured at 1.0 normalized depths are most suggestive of a quadrupole moment as they are extended in the vertical direction, compared to the best fit-results. As data collection artifacts only affect the horizontal direction, the vertical extension suggests quadrupolar-type residuals would be present if positioning were improved.

Positioning inaccuracy is the result of navigation artifacts induced by inaccurate coordination of fiducial marking with the start and end of each line. Such artifacts introduced both random and systematic errors into the in-line positioning. These errors manifest as a visual segmentation of the anomaly by shifting, stretching, and compression parallel to the line direction (east-west). Such spatial shifting can destroy or create complex field patterns, when the unshifted model is subtracted from the shifted data. Low pass filtering of the data followed by fitting and subtraction Filtering of the results would yield a low pass of the corrupted residual. In this case, systematic errors are worse than the random errors investigated in the theoretical analysis, however, as such systematic errors are strongly tied to the data collection method, and because alternatives which would not produce such errors are available, this should not be considered a limiting factor of the method. Cross-line positioning was accurate to within .25 inch. Errors of in-line positioning have been evaluated and we are confident that processing can be applied to minimize these effects and to enhance the quadrupolar-type residuals, alternatively, a more accurate dynamic-positioning mechanism can be designed: this was not possible within the constraints of the current effort. Of course, the simplest means of eliminating such errors would be to collect the data at each point with a stationary sensor. We had originally planned to do this, however, tests showed that the increased sampling required for the quadrupolar-type fields and the number of planes required for collection made stationary point-collection infeasible within the time and budget constraints of this project.

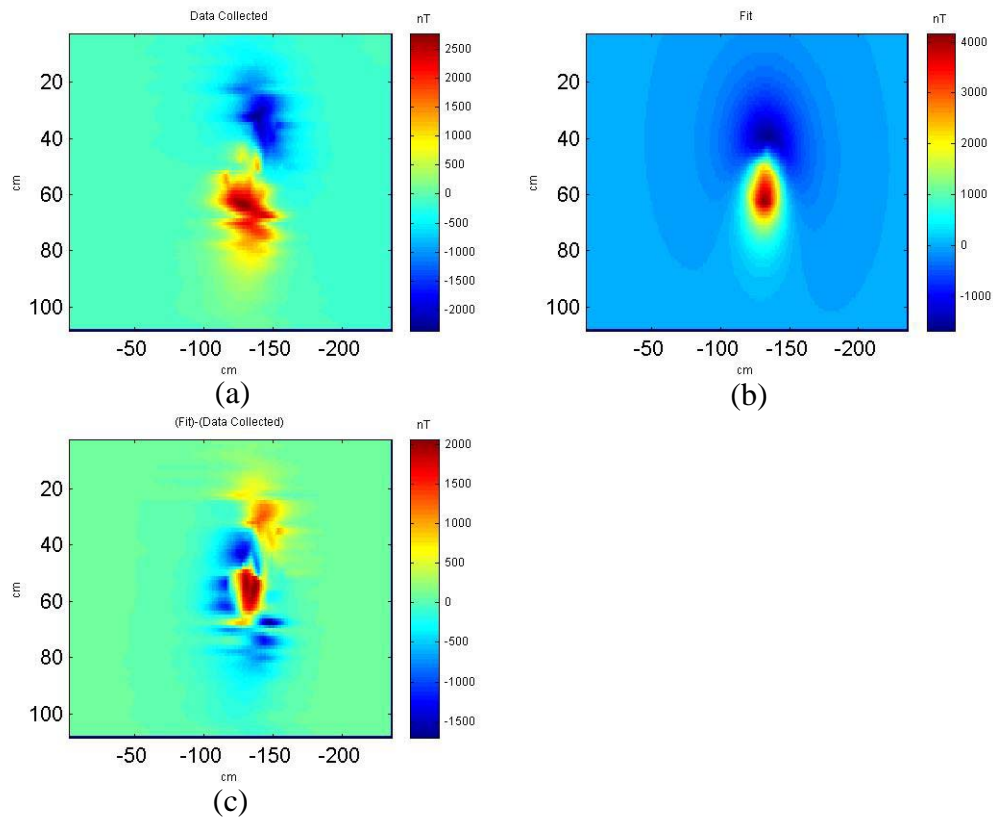


Figure 40. Data collected over the large IROS piece, from the base of a 155 mm projectile, at a height of .5 normalized depths, appears in (a) with the fit in (b). The residual appears in (c). Despite the complex residual, which reflects a substantial component caused by linear positioning errors, it is apparent that the vertical extent of contours around the original anomaly are extended relative to the best fit-result: this suggests that there will be a quadrupolar-type residual if positioning can be improved. Horizontal positioning distortions do not affect the vertical extent of the anomaly.

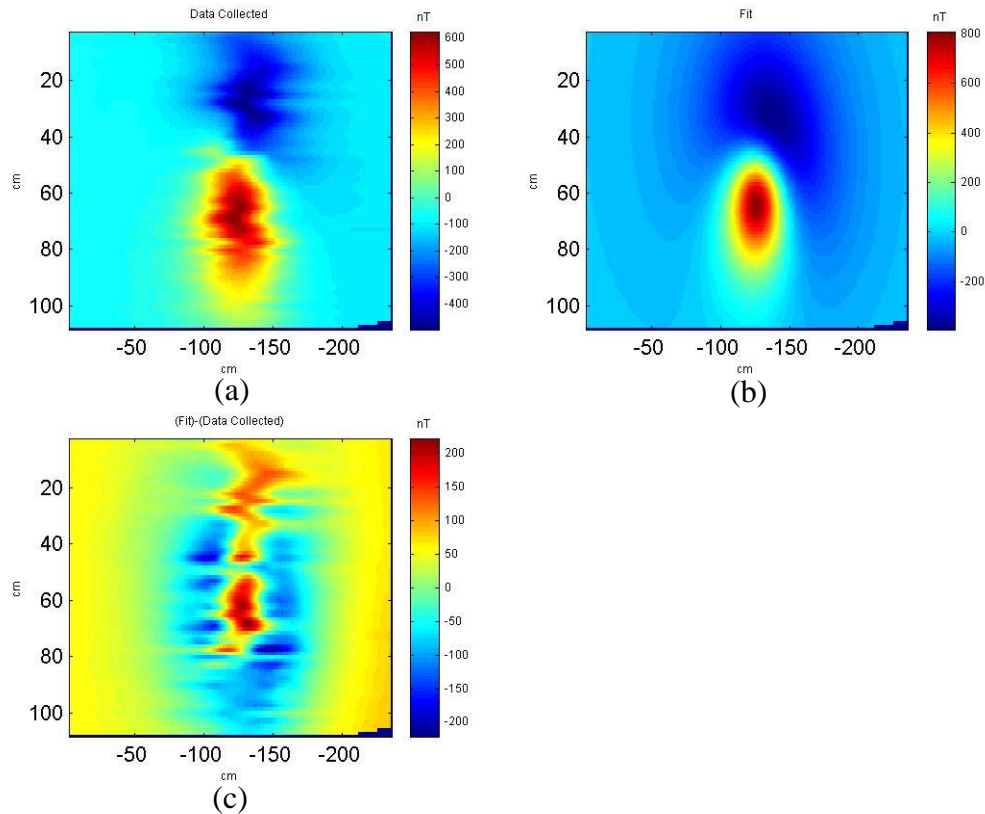


Figure 41. Data collected over the large IROS piece, from the base of a 155 mm projectile, at a height of 1.0 normalized depths, appears in (a) with the fit in (b). The residual appears in (c). Despite the complex residual, which reflects a substantial component caused by the positioning errors, it is apparent that the vertical extent of contours around the original anomaly are extended relative to the best fit result: this suggests that there will be a quadrupolar-type residual if positioning can be improved. Horizontal positioning distortions do not affect the vertical extent of the anomaly.

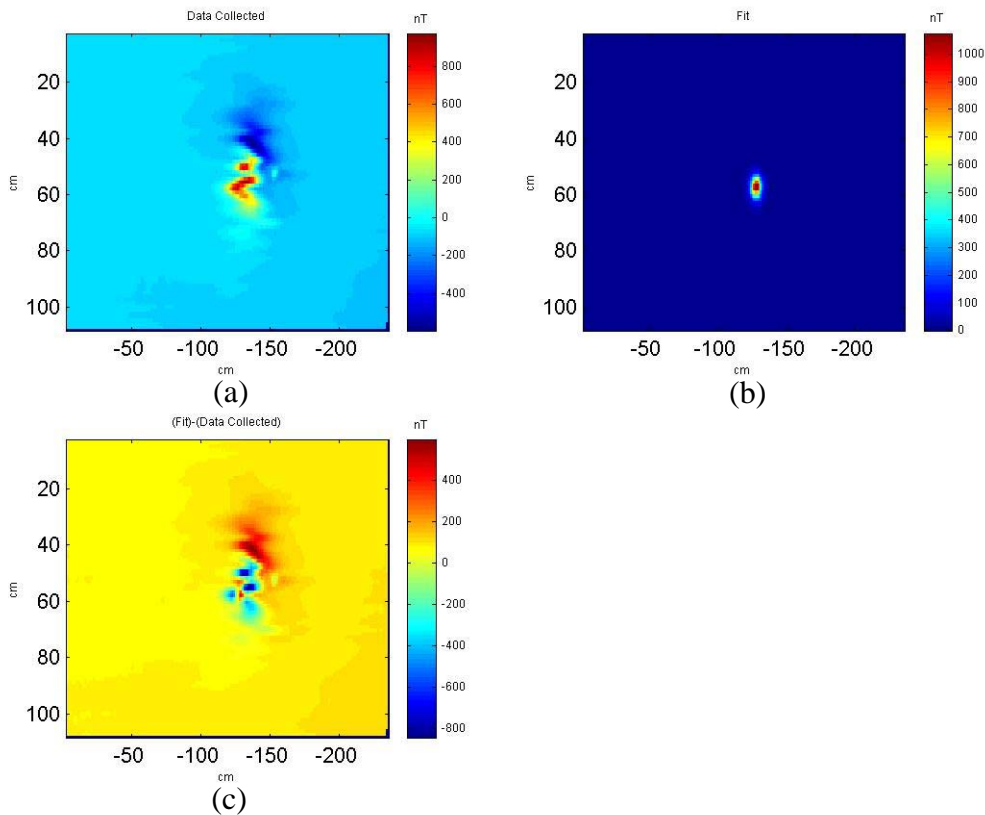


Figure 42. Data collected over the small IROS piece (about the same body length as a 20 mm), from the nose section of a 155 mm projectile, at a height of 1.0 normalized depths, appears in (a) with the fit in (b). The residual appears in (c). Despite the complex residual, which reflects a substantial component caused by the positioning errors, it is apparent that the vertical extent of contours around the original anomaly are extended relative to the best fit-result: this suggests that there will be a quadrupolar-type residual if positioning can be improved. In this case, a poor fit may have been obtained as a direct result of the target-anomaly complexity: corrections to the anomaly would aid in verifying this. Horizontal positioning distortions may be sufficient to affect the vertical extent of the anomaly.

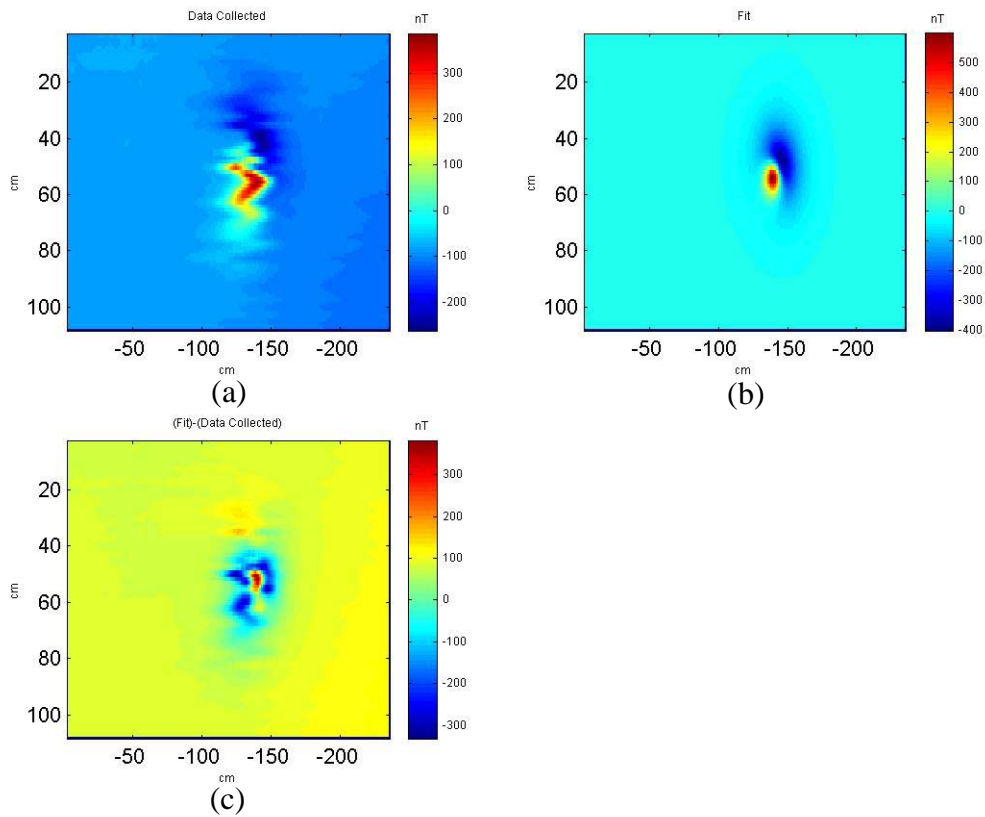


Figure 43. Data collected over the small IROS piece (about the same body length as a 20 mm), from the nose section of a 155 mm projectile, at a height of $3/2$ normalized depths, appears in (a) with the fit in (b). The residual appears in (c). Despite the complex residual, which reflects a substantial component caused by the positioning errors, it is apparent that the vertical extent of contours around the original anomaly are extended relative to the best fit result: this suggests that there will be a quadrupolar-type residual if positioning can be improved. Horizontal positioning distortions do not significantly alter the vertical extent of the anomaly, at this height.

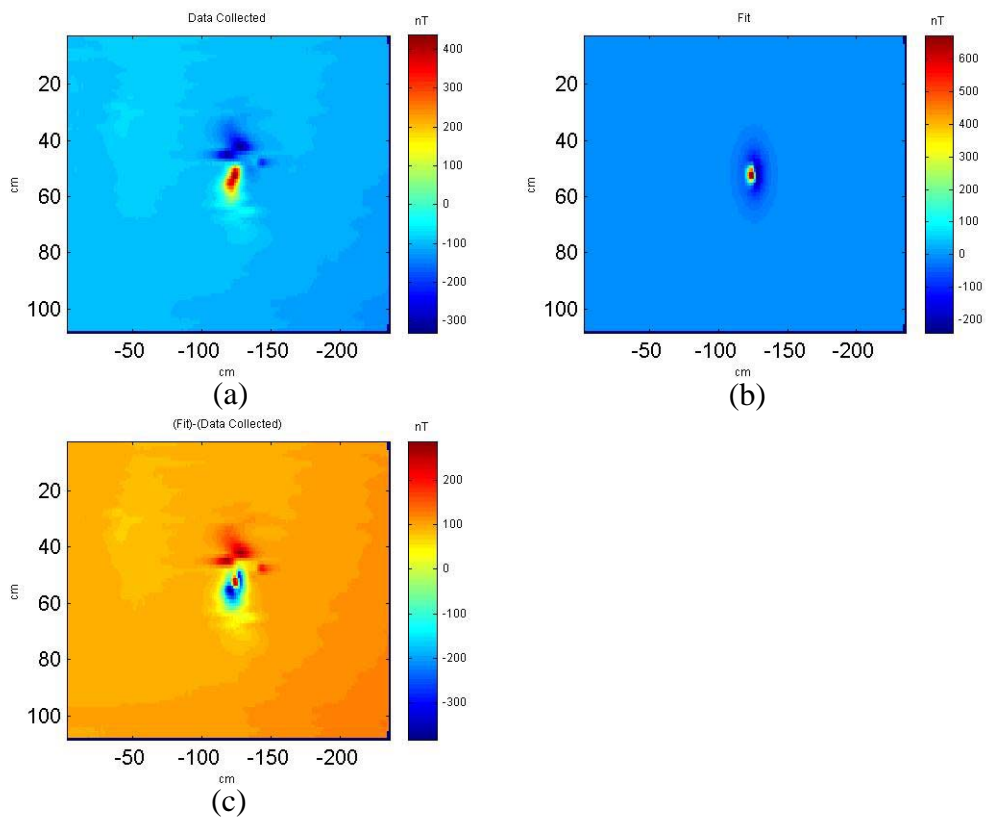


Figure 44. Data collected over the 20 mm projectile, at a height of 1 normalized depth, appears in (a) with the fit in (b). The residual appears in (c). Despite the complex residual, which appears to reflect an unexpectedly complex component of the original data and may also reflect a component caused by the positioning errors, it is apparent that the vertical extent of contours around the original anomaly are extended relative to the best fit result: this suggests that there will be a quadrupolar-type residual if the artifacts are reduced. Alternatively, the best fit result may be dominated by anomaly complexity arising from positioning artifacts. The presence of a complex residual for a UXO would be significant as it would show that the actual geometry violates standard symmetry assumptions sufficiently to produce measurable quadrupolar-type fields. Such fields were predicted by our earlier theoretical modeling results from two other UXO: a 80-mm and a 155-mm. Horizontal positioning distortions may be sufficient to affect the vertical anomaly extent.

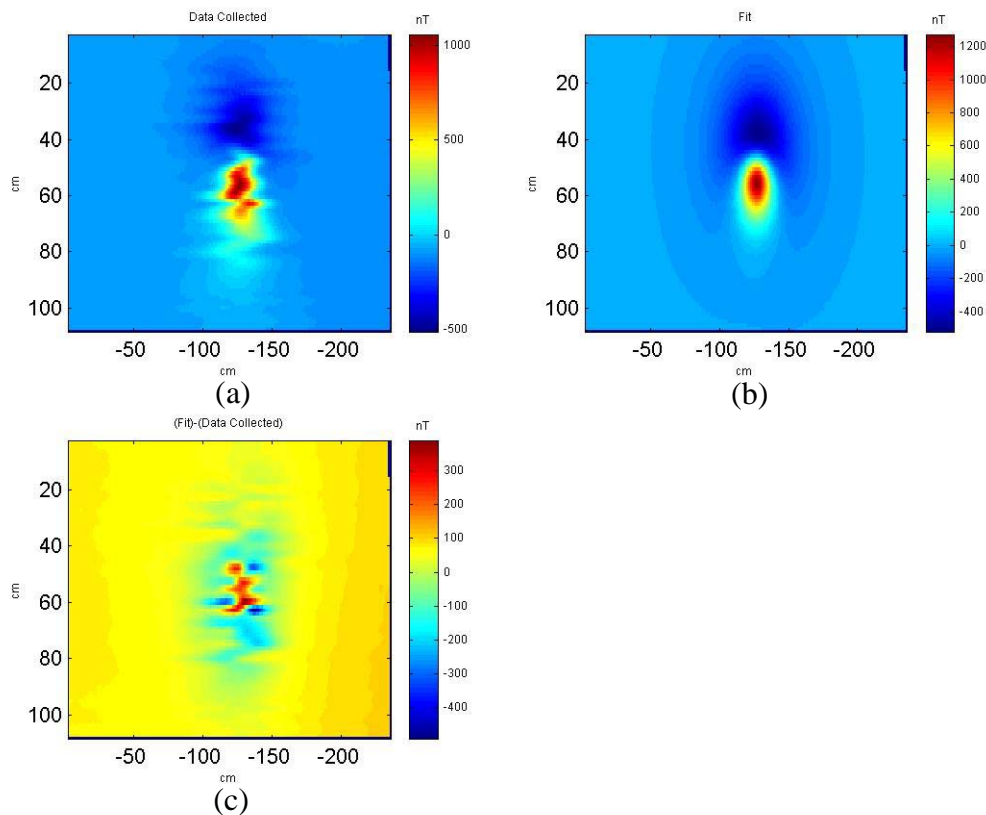


Figure 45. Data collected over the 57 mm projectile, at a height of 1.0 body lengths, appears in (a) with the fit in (b). The residual appears in (c). Despite the complex residual, which reflects a substantial component caused by the positioning errors, it is apparent that the vertical extent of contours around the original anomaly are extended relative to the best fit-result: this suggests that there will be a quadrupolar-type residual, if positioning can be improved. The presence of such a residual for a UXO would be significant as it would show that the actual geometry violates standard symmetry assumptions sufficiently to produce measurable quadrupolar-type fields. Such fields were predicted by our earlier theoretical modeling results from two other UXO: an 80-mm and 155-mm projectile. Horizontal positioning distortions do not affect the vertical extent of the anomaly.

7 Findings

We have eliminated the geometrically simplifying assumptions of standard geometric-dipole models and, for the first time, modeled the full geometric complexity of UXO and ordnance-related scrap. This effort has allowed us to identify two subsets of ordnance related scrap: regular (ROS) and irregular (IROS), a byproduct of the modeling that was not in the original scope of this effort. This permits investigation of subcomponents of UXO that are commonly found on UXO remediation sites, but which have heretofore not been specifically considered in terms of a distinct class of objects with a potential for discrimination that may differ from that of the original UXO. The fields of ROS items can be substantially non-dipolar, depending upon the shape of the subcomponent. Further information is required on the expected or actually identified modes of failure and the specific subcomponent geometries, and physical properties, expected, before the

effects of these regular scrap items on discrimination capabilities can be assessed. Additionally, the prevalence of ROS, in comparison to irregular ordnance scrap (IROS), and the subset of it that might be considered UXO may obviate any need to further evaluate these items.

Our modeling and inversion results, for the two UXO and two IROS investigated here, show that standard geometric dipole models are too restrictive and limit the information derivable from both the scrap and the UXO, in terms of discrimination. A more general understanding of the fields, and a viable method for improved discrimination, is obtained by allowing for broken symmetries. These arise when geometrical restrictions on the target, imposed by standard dipole models, are eliminated. Specifically:

1. Modeling indicates that the non-dipole fields of the 2 irregular ordnance scrap (IROS), derived from the 2 UXO, show quadrupolar-type residual anomalies, after subtraction of the dipole component, and that this quadrupolar-type field is measurable and robust to sensor and positioning noise. The existence and detectability of the quadrupolar fields of scrap has not been previously identified.
2. Modeling indicates that the non-dipole fields of the 2 UXO show quadrupolar-type residual anomalies, after subtraction of the dipole component, and that this quadrupolar-type field is measurable and robust to sensor and positioning noise. The existence and detectability of the quadrupolar fields of UXO has not been previously identified.
3. Comparison of quadrupolar-type residual fields from scrap with those from the corresponding UXO indicates that the scrap is enriched in the quadrupolar-type field as a fraction of the total field at shallow normalized depths (depth/body length):
 - a. For the 80-mm projectile and the IROS derived from its body, we found the quadrupolar type residual is about 20% of the IROS field, whereas it is about 10% of the intact ordnance field, at .5 normalized depths.
 - b. For the 155-mm projectile and the IROS representing a substantial portion of its body, we found the quadrupolar type residual is still about 27% of the IROS field, whereas it is about 16% of the intact ordnance field, at .5 normalized depths.
4. Comparison of quadrupolar-type residual fields from scrap with those from the corresponding UXO indicates that the scrap field is stronger than the UXO field at equivalent normalized depths and differ in strength and/or spatial signature at equivalent absolute depth:
 - a. For the 80-mm projectile and the IROS derived from its body, we found the quadrupolar type residual of the IROS is about 10 times that of the intact UXO, at equivalent normalized depths. At equal absolute depth, we found the quadrupolar type residual of the much smaller IROS is much weaker than that of the intact UXO, and differs in spatial signature.
 - b. For the 155-mm projectile and the IROS representing a substantial portion of its body, we found the quadrupolar type residual of the IROS is about 3 times that of the intact UXO, at equivalent normalized depths. At equal absolute depth, we found the quadrupolar type residual of the comparably sized IROS remains about 1.4 times that of the intact UXO, and differs in

spatial signature: this provides a potential discriminator between the intact UXO and even large portions of its body, a level of discrimination that is not even being considered presently.

5. Interaction of one or more noise sources with the non-dipole field of an item is a complex process as the fields must be derived indirectly from the measurements, and noise may contaminate this initial step. We have investigated some specific practical cases in an attempt to provide insight into real field performance and this has demonstrated that despite the complexity, the non-dipole signatures investigated are robust to typical noise sources over a range of depths of interest. Specifically, the non-dipole field of an IROS comprising a substantial portion of the body of a 155 mm projectile can be detected to about 1.5 body lengths, in combined sensor and positioning noise of 5 nT and 4 cm standard deviation, respectively. In contrast, IROS comprising about half the main body of length of an 80-mm projectile can be detected to about 1.5 body lengths, in combined sensor and positioning noise of 1 nT and 1 cm standard deviation, respectively. Simple filtering aids detection and increases the range. These numerical results were not borne out in the field data, which showed poor resolution of quadrupolar-type anomalies. As discussed on p.42, the field data incurred random and systematic positioning errors along data collection lines. These combined error sources cause data shifts that can destroy or create complex field patterns, when the unshifted model is subtracted from the shifted data. The apparent lack of corroboration of noise sensitivity results between the numerical modeling and the field collection should not be viewed as a failing of the method but, rather, as a failing of the field positioning method. Specifically, alternatives which would not produce such errors are available; the simplest of these would be to collect data at each point with a stationary sensor. Obviously, tradeoffs of time and cost would militate against this particular positioning method as a viable field methodology.
6. Sampling is an important practical concern for any feasible discrimination methodology and our investigations have shown that the practical implementation of a non-dipole discrimination methodology will require a tradeoff of time (to achieve the desired sampling density) versus the quadrupolar-type anomaly detection limit (for the smallest target of interest, and at the shallowest depth of interest), considering the possible range of target anomaly sizes and depths. We have specifically found that field sampling requirements for implementing a quadrupolar-type scrap-discrimination will require much more stringent sampling than is currently being applied even in "high resolution" field surveys, for example, the 80-mm IROS, which is 11.9 cm long and about 6 cm across, requires a sample spacing of less than 3 cm to unambiguously recover the spatial spectrum at .5 normalized depths (about 6 cm). Sampling requirements become less stringent as the depth increases and the targets get bigger, and vice versa. UXO expected at a given site will determine the tradeoffs taken. Additionally, the sampling criteria may explain why the quadrupolar-type fields have not been previously recognized in field data: they were aliased. In addition to the spatial sampling requirements we have found that a sampling window of 3x3m is adequate to recover all but the deepest residual anomalies (below about 2 normalized depths) from the largest UXO (155-mm).

7. Field data collection produced data of lower quality than expected, however, the intact 57-mm projectile and IROS from the base of a 155, produce residual fields which suggest that quadrupolar-type residuals would be seen if positioning of the field data were improved. The smaller targets also suggest quadrupolar-type fields but the effects of data collection artifacts are more significant for these targets. Evaluation of the data indicates that linear shifting, stretching, and compression are the causes of data degradation: these can be improved by further processing or recollection with minor improvements in the collection system: both of these are beyond the scope of the present effort.

8 Conclusions:

1. Modeling the magnetostatic fields of an 81-mm projectile, a 155-mm projectile, and 2 irregular ordnance scrap pieces derived from the respective projectile bodies, using the full three-dimensional geometric complexity of each object, provides new physical insight and forms the basis for a new UXO discrimination method based upon the non-dipole fields. These fields become relevant when geometrical restrictions on the target, imposed by standard dipole models, are eliminated and previously required symmetries are broken. Such broken symmetry is characteristic of scrap and is shown here to also apply to UXO.
2. Following removal of the dipole field, the residuals from each of the targets, shows a quadrupolar spatial signature, and is well approximated by a range decay with an exponent of -4, over depths ranging from .5 to 3 body lengths.
3. Investigation of the quadrupolar-type residual fields indicates that these fields are measurable, are enhanced in the scrap relative to the UXO, are robust to typical noise sources, and provide differentiable signatures for discrimination against scrap at depths up to 3 body lengths.
4. Prior results for UXO, indicating weak excitation of the higher moments, were not corroborated in this investigation. As a result, simply using a threshold magnitude of the quadrupolar field as a means of discriminating scrap from UXO is not feasible, however; distinctive signatures of quadrupolar-type residuals, from UXO, show great potential. Specifically, these signatures may not only provide a means of discriminating against small scrap items but even against scrap that is a substantial portion of the original shell body. Additionally, in contrast to our original expectation of negligible quadrupolar-type fields in UXO, the distinctive signatures of residual fields from UXO may provide a means of discriminating between different UXO.
5. Sampling criteria are an important consideration for the successful detection of quadrupolar fields and are also an important economic consideration. Sampling will be governed by the smallest item to be discriminated, at the shallowest depth and this generally places constraints upon sampling that are well beyond those achieved in standard surveys (a few cm): tradeoffs in collection time and signature quality can be made on a site by site basis: the method is presently best applied as a cued discrimination method.
6. Field investigations suffered from inadequate positioning and produced only suggestions of quadrupolar fields: rigorous validation of the modeling results is an outstanding issue that may be resolved by further processing the existing data, and/or collecting new data.
7. The potential for discrimination using the quadrupolar-type signatures, identified for the first time, in this study is significant: as we have investigated only

horizontal UXO and scrap, the quadrupolar field from the UXO is expected to be maximized on a horizontal plane and diminished when the UXO is not horizontal, due to the tensor character of the quadrupolar excitation. Accordingly, we expect that the results reported here represent the “worst case” scenario for differentiating UXO from scrap. Alternatively, one could argue that it represents the best case scenario for differentiating among different UXO, but this was not an intended objective of this effort. In contrast to the UXO, we expect that the irregular scrap will exhibit enhanced quadrupolar-type fields over all orientations, thereby providing a robust discrimination against scrap, which was the primary objective of this effort.

9 Recommendations:

The results of this SEED effort are very promising for scrap discrimination as they indicate that non-dipole fields of modeled scrap are: measurable, stronger than the non-dipole fields of modeled UXO, robust to noise sources, and exhibit characteristic differences that serve to distinguish scrap from UXO, at depths of up to a few body lengths. Additionally, because the modeled UXO also exhibit quadrupolar-type residuals, and these residuals have characteristic signatures, it may also be possible to distinguish different UXO. We recommend that these results be further investigated using additional forward modeling, development of new inversion/interpretation methods, and, most importantly, field data collection to provide indisputable evidence for the predominance of the quadrupolar-type residual fields at up to a few body lengths.

10 References

Grimm, R.E., “Time Domain Measurements and Modeling of UXO”, UXO Forum Conference Proceedings, New Orleans, LA, 2001.

D.A. Lieblich, D. Reidy, and J.E. Foley, “Use Of Groundtruth Information to Improve the Effectiveness of Geophysical Analysis at Umatilla Army Depot,” UXO Forum Conference Notebook, Anaheim, CA, May 5-7, 1998.

J.E. McFee and Y. Das, “A multipole Expansion model for compact ferrous object detection,” ANTEM, 1990, pp.633-638.